

1 **Synchronous emplacement of the anorthosite
2 xenolith-bearing Beaver River diabase and one of the
3 largest lava flows on Earth**

4 **Yiming Zhang¹, Nicholas L. Swanson-Hysell¹, Mark D. Schmitz², James D.
5 Miller Jr.³, Margaret S. Avery^{1,4}**

6 ¹Department of Earth and Planetary Science, University of California, Berkeley, California, USA

7 ²Department of Geosciences, Boise State University, Boise, Idaho, USA

8 ³Department of Earth and Environmental Sciences, University of Minnesota, Duluth, Minnesota, USA

9 ⁴U.S. Geological Survey, Moffett Field, California, USA

10 **Key Points:**

- 11 • New geochronology on an anorthosite xenolith tightly constrain the timing of the
12 Beaver River diabase intrusions.
- 13 • Paleomagnetic and geochronological data support that the Beaver River diabase
14 is comagmatic with the very high volume Greenstone Flow.
- 15 • Wide conduits of magma to the surface are indicated by large anorthosite xeno-
16 liths.

17 **Abstract**

18 New geochronologic and paleomagnetic data from the North American Midcontinent Rift
 19 (MCR) reveal the synchronous emplacement of the Beaver River diabase, the anorthosite
 20 xenoliths within it, and the Greenstone Flow — one of the largest lava flows on Earth.
 21 A U-Pb zircon date of 1091.83 ± 0.21 Ma (2σ) from one of the anorthosite xenoliths is
 22 consistent with the anorthosite cumulate forming as part of the Midcontinent Rift and
 23 provides a maximum age constraint for the Beaver River diabase. Paired with the min-
 24 imum age constraint of a cross-cutting Silver Bay intrusion (1091.61 ± 0.14 Ma; 2σ) these
 25 data tightly bracket the age of the Beaver River diabase to be 1091.7 ± 0.2 Ma (95% CI),
 26 coeval with the eruption of the Greenstone Flow (1091.59 ± 0.27 Ma; 2σ) — which is
 27 further supported by indistinguishable tilt-corrected paleomagnetic pole positions. Geochrono-
 28 logical, paleomagnetic, mineralogical and geochemical data are consistent with a hypoth-
 29 esis that the Beaver River diabase was the feeder system for the Greenstone Flow. The
 30 large areal extent of the intrusives and large estimated volume of the volcanics suggest
 31 that they represent a rapid and voluminous *ca.* 1092 Ma magmatic pulse near the end
 32 of the main stage of MCR magmatism.

33 **1 Introduction**

34 The North American Midcontinent Rift (MCR) is a *ca.* 1.1 Ga large igneous province
 35 for which there is excellent exposure of both the intrusive and extrusive components in
 36 the Lake Superior region (Fig. 1). An exceptional feature within the Midcontinent Rift
 37 is the occurrence of large anorthosite xenoliths within a diabase sill and dike network
 38 known as the Beaver River diabase that outcrops in northeastern Minnesota, USA, as
 39 part of the Beaver Bay Complex (Fig. 1). The anorthosite xenoliths range in size from
 40 centimeter-scale megacrysts to meter-scale, decimeter-scale and even >150 meter-scale
 41 blocks (Fig. 2; Morrison et al. (1983); Grout (1939)). A particularly large anorthosite
 42 xenolith is exposed at Carlton Peak in the eastern Beaver Bay Complex with minimum
 43 dimensions of 180×240 meters (Fig. 1, 2; Boerboom et al. (2006)). In the southern Beaver
 44 Bay Complex, a large anorthosite xenolith near Corundum Point has dimensions of 180
 45 $\times 230$ meters while one exposed at Split Rock Point has dimensions of 180×260 me-
 46 ters (Boerboom, 2004). To be able to accommodate such large xenoliths during magma
 47 ascent, the Beaver River diabase conduits must have been of at least the width of the
 48 anorthosite short axis diameters. Such wide conduits in these near-surface intrusions sug-

49 gest high magma flux rates and make it likely that the magma extruded to the surface
 50 — feeding voluminous lava flows.

51 Miller and Chandler (1997) emphasized the composite nature of the Beaver River
 52 diabase network and Silver Bay intrusions (Fig. 1), which are locally marked by abrupt
 53 transitions to progressively more evolved lithologies. Furthermore, Miller and Chandler
 54 (1997) documented geochronologic, geochemical and structural evidence to support the
 55 notion that the diabase network may have served as principal feeder conduits to lava flows
 56 including parts of the Portage Lake Volcanics on the Keweenaw Peninsula and Isle Royale
 57 of Michigan (Fig. 1). To more directly test this inferred intrusive-extrusive correlation,
 58 Doyle (2016) compared the mineralogical, textural, and geochemical attributes and the
 59 composite lithologic nature of the Beaver River diabase against those of the Greenstone
 60 Flow, the largest lava flow within the Midcontinent Rift and one of the largest lava flows
 61 on Earth (Fig. 3). Doyle (2016) documented remarkable similarities in petrography, min-
 62 eral chemistry, whole rock geochemistry, and interpreted lithologic zonation between the
 63 Beaver River diabase intrusions in northern Minnesota and the Greenstone Flow on both
 64 Isle Royale and Keweenaw Peninsula. Based on the interpreted feeder system being in
 65 northern Minnesota, Doyle (2016) estimated the full areal extent of the Greenstone Flow
 66 to be $\sim 20000 \text{ km}^2$ and its volume to be between 2000 and 6000 km^3 (Fig. 3).

67 A comagmatic relationship between the Beaver River diabase and the Greenstone
 68 Flow is consistent with the similar $^{207}\text{Pb}/^{206}\text{Pb}$ dates developed from a granophytic fer-
 69 rogabbro within the Beaver Bay Complex ($1095.8 \pm 1.2 \text{ Ma}$, Paces and Miller (1993))
 70 and the Greenstone Flow ($1094.0 \pm 1.5 \text{ Ma}$, Davis and Paces (1990)). The relatively large
 71 uncertainties provided by the existing $^{207}\text{Pb}/^{206}\text{Pb}$ geochronology provide less precise
 72 estimates of the temporal relationships between these rapid events than is possible with
 73 modern methods. Modern-day U-Pb geochronology techniques for chemical abrasion iso-
 74 tope dilution-thermal ionization mass spectrometry (CA-ID-TIMS) allow high-precision
 75 $^{206}\text{Pb}/^{238}\text{U}$ dates to be developed from chemically abraded zircon crystals (Mattinson,
 76 2005). Studies utilizing these methods on Midcontinent Rift volcanic and intrusive rocks
 77 have shown that the analytical uncertainties on weighted mean $^{206}\text{Pb}/^{238}\text{U}$ dates of mul-
 78 tiple chemically abraded single zircons can be $\sim 200 \text{ kyr}$, an order of magnitude smaller
 79 than previous dates that are based exclusively on the $^{207}\text{Pb}/^{206}\text{Pb}$ system (Fairchild et
 80 al., 2017; Swanson-Hysell et al., 2019, 2020). These $^{206}\text{Pb}/^{238}\text{U}$ dates are also consid-
 81 ered to be more accurate than systematically older $^{207}\text{Pb}/^{206}\text{Pb}$ dates (Schoene et al.,

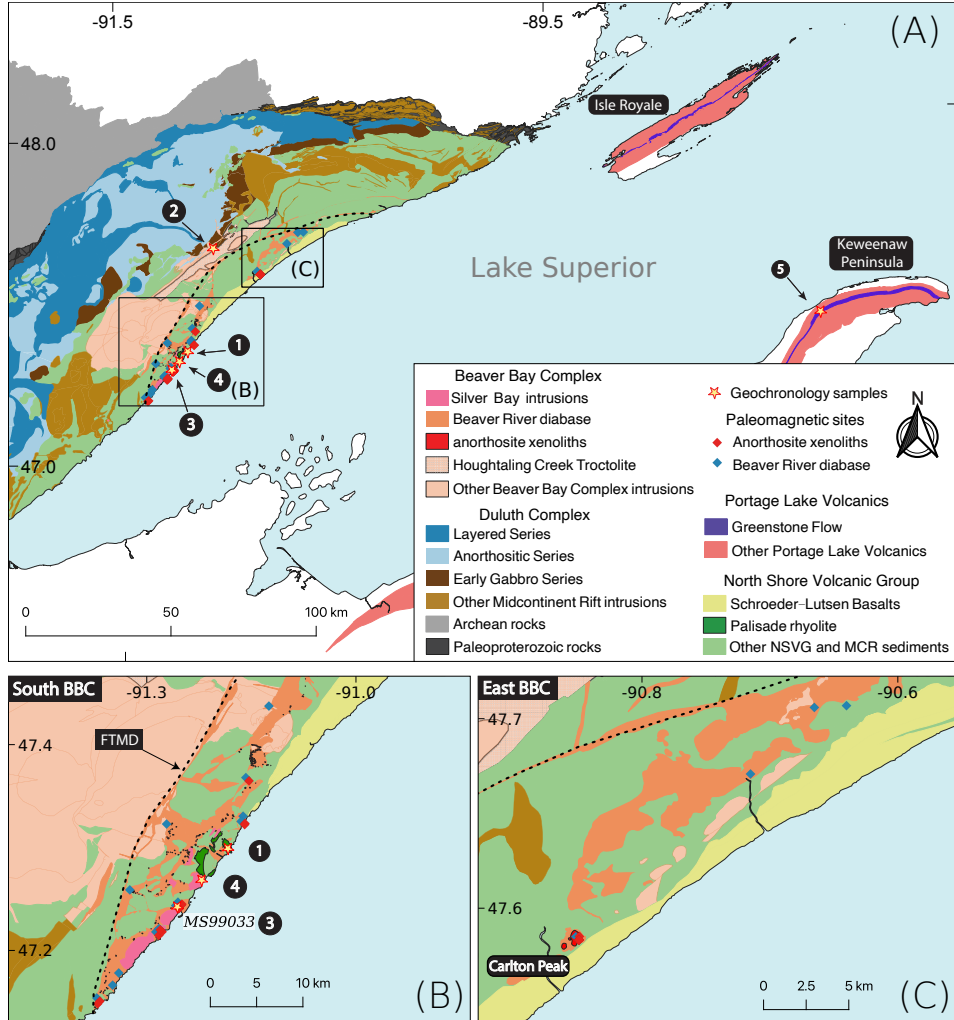


Figure 1: (A) Geologic map of exposures of Midcontinent Rift volcanics and intrusives in the western Lake Superior region. The Greenstone Flow (purple) of the Portage Lake Volcanics (red) outcrops throughout the Keweenaw Peninsula and Isle Royale. (B) Regional map of paleomagnetic and geochronologic sites in the southern Beaver Bay Complex (south BBC). Note that paleomagnetic site AX16 and geochronology sample MS99033 are from the same anorthosite xenolith. The geochronology sample numbers in (A) and (B) correspond to those in Fig. 4. (C) Regional map of paleomagnetic sites in the eastern Beaver Bay Complex (east BBC). The xenolith at Carlton Peak is >100 meters in diameter. The younger Schroeder-Lutsen basalt of the North Shore Volcanic Group (NSVG) is lying unconformably atop the Beaver River diabase and other NSVG units. The nomenclature of the “southern” and “eastern” Beaver Bay Complex follows Miller and Chandler (1997). FTMD - Finland tectonomagmatic discontinuity, traced out by the dashed black line. Bedrock geology is from Miller et al. (2001) and Jirsa et al. (2011).

82 2006). Such $^{206}\text{Pb}/^{238}\text{U}$ dates indicate that the massive Layered Series and Anorthositic
 83 Series rocks of the Duluth Complex were emplaced in \sim 500 kyr *ca.* 1096 Ma (Swanson-
 84 Hysell et al., 2020).

85 In this work, we use a new $^{206}\text{Pb}/^{238}\text{U}$ zircon date for an anorthosite xenolith hosted
 86 within the Beaver River diabase, in conjunction with $^{206}\text{Pb}/^{238}\text{U}$ dates from a Silver Bay
 87 intrusion and the Greenstone Flow (Fig. 1; Fairchild et al. (2017)), to evaluate the tim-
 88 ing of emplacement of the Beaver River diabase, and the hypothesized intrusive-extrusive
 89 correlation between the Beaver River diabase and the Greenstone Flow.

90 Paleomagnetic data can also provide chronological constraints on rock units. Lau-
 91 rentia experienced a period of rapid latitudinal plate motion during rift development (Swanson-
 92 Hysell et al., 2009). A synthesized apparent polar wander path (APWP) based on the
 93 Midcontinent Rift volcanic rocks indicates that motion exceeded 20 cm/yr (Swanson-
 94 Hysell et al., 2019), faster than the maximum speed of India of \sim 17 cm/yr during the
 95 Cenozoic (van Hinsbergen et al., 2011). This motion resulted in significant differences
 96 in pole positions recorded by Midcontinent Rift rocks that were emplaced a few million
 97 years apart (Swanson-Hysell et al., 2019). In this study, we present paleomagnetic data
 98 from the anorthosite xenoliths and the host Beaver River diabase. Data from the xeno-
 99 liths give equivalent directions to the host diabase (Figs. 7, 8), indicating that they were
 100 heated above the Curie temperature of magnetite and acquired a thermal remanent mag-
 101 netization when they cooled within the diabase. This thermal history is consistent with
 102 thermal diffusion modeling of the xenoliths (Fig. 9). The paleomagnetic data can be com-
 103 compared to data from the Greenstone Flow to further test the hypothesis that they are syn-
 104 chronous. The resulting paleomagnetic pole positions can also be compared to the syn-
 105 thesized Laurentia APWP to obtain chronological constraints (Fig. 8).

106 Here, by integrating the geochronologic and paleomagnetic perspectives with pre-
 107 vious lithologic and geochemical analyses (Miller & Chandler, 1997; Doyle, 2016), we show
 108 that these data are consistent with the Beaver River diabase network acting as the feeder
 109 system for the Greenstone Flow of the Portage lake Volcanics. Alternatively, they could
 110 both be the distinct manifestations of magmatism from a similar source. Regardless, their
 111 shared geochemical signatures and the inference of giant magma conduits that transported
 112 large anorthosite xenoliths characterize a period of *ca.* 1092 Ma voluminous magmatic
 113 activity (based on $^{206}\text{Pb}/^{238}\text{U}$ zircon dates; Fig. 1).

114 **2 Geologic Setting**115 **2.1 Beaver Bay Complex and Related Rocks of NE Minnesota**

116 The North American Midcontinent Rift (MCR) is a failed intracontinental rift where
 117 protracted magmatic activity lasted from *ca.* 1109 Ma to *ca.* 1084 Ma (Swanson-Hysell
 118 et al., 2019). Midcontinent Rift rocks extensively outcrop in today's Lake Superior re-
 119 gion, with the total extent traceable by arcuate magnetic and gravity anomalies that ex-
 120 tend to the southwest to Kansas, and to the southeast, to southern Michigan (Hinze &
 121 Chandler, 2020). Previous studies have divided magmatic activity in the rift into four
 122 stages based on interpreted changes in relative magmatic volume and the nature of mag-
 123 matism: early (\sim 1109–1104 Ma), latent (\sim 1104–1098 Ma), main (\sim 1098–1090 Ma) and late
 124 (\sim 1090–1083 Ma) (Vervoort et al., 2007; Heaman et al., 2007; Miller & Nicholson, 2013).
 125 In northeastern Minnesota, the Early Gabbro Series and the Felsic Series rocks of the
 126 Duluth Complex and reversed-polarity lavas of the lower North Shore Volcanic Group
 127 were emplaced during the early stage. The more voluminous Duluth Complex Layered
 128 Series and the plagioclase-rich Anorthositic Series, together with an associated \sim 8 km
 129 thick extrusive volcanic sequences of the North Shore Volcanic Group (NSVG), were rapidly
 130 emplaced about 10 myr later at *ca.* 1096 Ma during the main stage (Paces & Miller, 1993;
 131 Swanson-Hysell et al., 2020).

132 The Beaver Bay Complex, which sits stratigraphically above the Duluth Complex,
 133 is another intrusive complex that resulted from main stage magmatism. The exposed
 134 area of the Beaver Bay Complex is \sim 1000 km 2 where it has been mapped along the north-
 135 western shore of Lake Superior in northeastern Minnesota (Fig. 1). The Beaver Bay Com-
 136 plex is a multi-phase, composite intrusive complex that intrudes parts of the NSVG (Fig.
 137 1; Miller and Chandler (1997); Swanson-Hysell et al. (2020)). Distinct from the deep plu-
 138 tonic intrusions of the Duluth Complex, the majority of the Beaver Bay Complex is formed
 139 of hypabyssal intrusions that were emplaced as dikes and sills at shallow depths (Miller
 140 & Chandler, 1997). Most of the Beaver Bay Complex intrusions are dioritic to gabbroic
 141 in composition (Miller & Chandler, 1997). The main lithology of the Beaver River di-
 142 abase dikes and sills network within the Beaver Bay Complex is an ophitic olivine gab-
 143 bro (Fig. 2), but in wider areas of dikes and the upper parts of thick sills, this rock type
 144 can abruptly transition into intergranular olivine oxide gabbro, then into subprismatic
 145 (and commonly foliated) ferrogabbro, and finally into granophyric monzodiorite. The

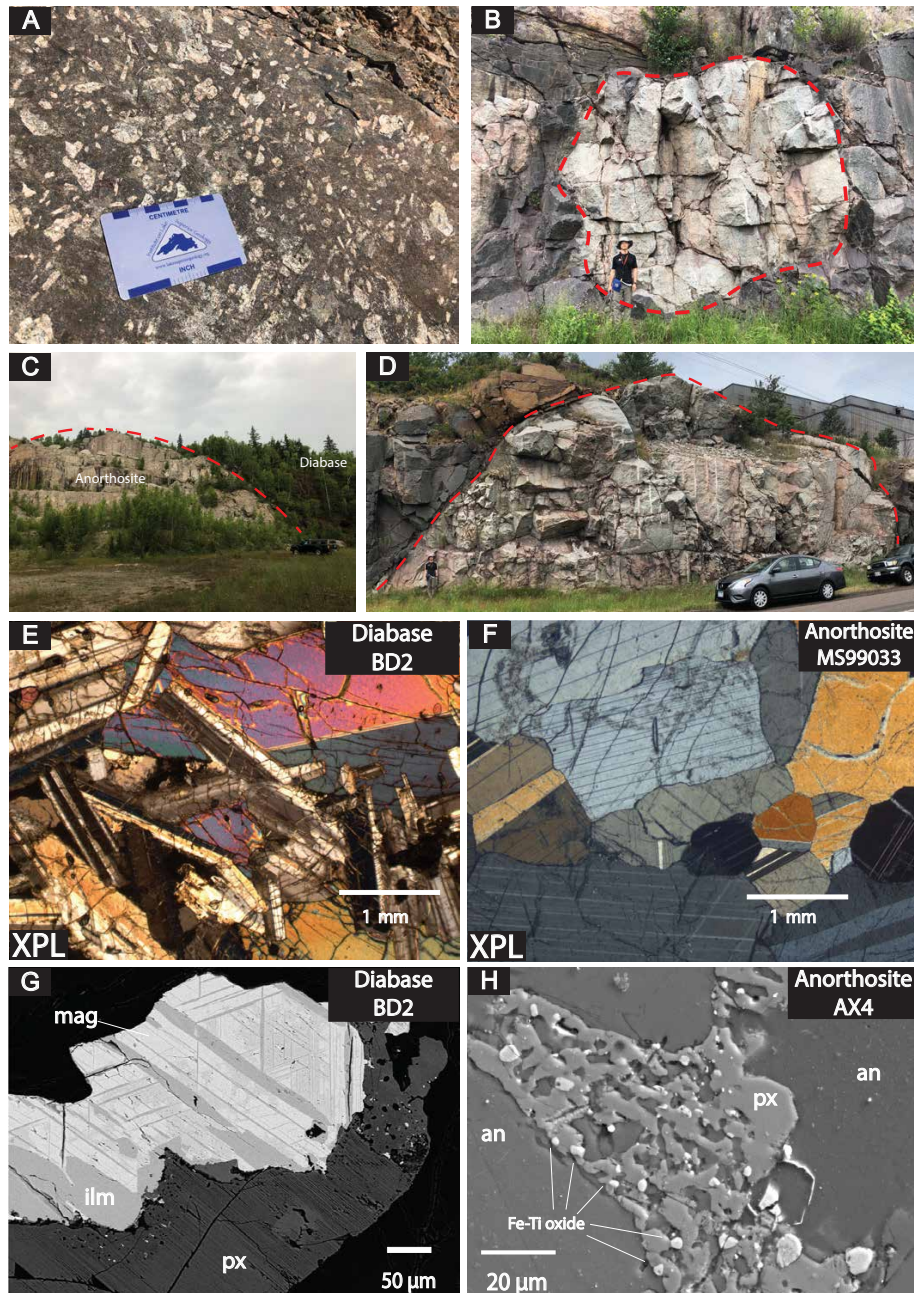


Figure 2: Field photographs and petrographic images of the Beaver River diabase and the anorthosite xenoliths within it. (A) Centimeter-sized plagioclase megacrysts in the diabase. (B) Rounded anorthosite xenolith with a diameter of ~ 7 meters fully enclosed within the diabase. (C) Exposure of a giant Carlton Peak anorthosite with a diameter >100 m. (D) 27.5 m diameter anorthosite xenolith sampled as paleomagnetic site AX16 and geochronology sample MS99033. (E) Cross polarized (XPL) image of the subophitic texture of diabase at site BD2 (pyroxene partially enclosing plagioclase). (F) XPL image of anorthosite geochronology sample MS99033. Plagioclase crystals exhibit both granoblastic texture and interlocking lath fabrics. (G) Backscattered electron (BSE) image of a large Fe-Ti oxide with titanomagnetite-ilmenite lamellae in Beaver River diabase site BD2. (H) BSE image of micron-sized Fe-Ti oxides exsolved from pyroxene between plagioclase crystals in anorthosite xenolith site AX4. an = anorthite; ilm = ilmenite; mag = magnetite; px = pyroxene.

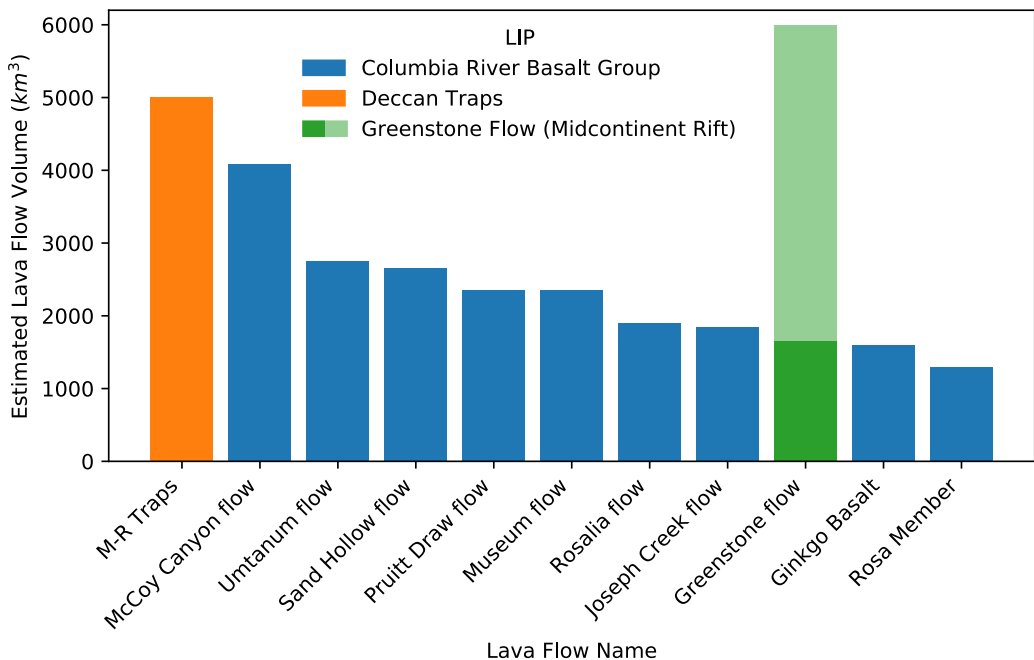


Figure 3: Bar plot of ten of the world's most voluminous single mafic lava flows currently known. With an estimated minimum volume of $\sim 1650 \text{ km}^3$ and likely volume as high as $\sim 6000 \text{ km}^3$, the Greenstone Flow from the 1.1 Ga Midcontinent Rift stands amongst the giant lava flows from the Deccan Traps and Columbia River basalts. M-R Traps = MahabaleshwarRajahmundry lava flow in the Deccan Traps. Volume estimates from Self et al. (2008), Bryan et al. (2010), Longo (1984), and Doyle (2016).

more evolved and later emplaced components of the Beaver River diabase network are commonly distinguished as the Silver Bay intrusions in the southern Beaver Bay Complex (Fig. 1). Overall being intermediate in composition, the Silver Bay intrusions lithologies range from ophitic olivine gabbro to ferrogranite (Shank, 1989). Field mapping by Miller et al. (1994) found intrusive relationships between the Silver Bay intrusions and the Beaver River diabase. Angular inclusions of the host Beaver River diabase within marginal zones of the Silver Bay intrusions led Miller and Chandler (1997) to interpret that the Silver Bay intrusions intruded after the diabase crystallized.

One distinctive feature of the Beaver River diabase is its inclusions of anorthositic xenoliths. In the southern part of the Beaver Bay Complex, the Beaver River diabase occurs as dikes and sills, typically including anorthosites with various sizes ranging from centimeters to over 150 meters (Figs. 1, 2; Grout (1939); Morrison et al. (1983)). The diabase in this region intrudes the Palisade rhyolite of the North Shore Volcanic Group

(Fig. 1), which has a $^{206}\text{Pb}/^{238}\text{U}$ date of 1093.94 ± 0.28 Ma (2σ analytical uncertainty is presented for CA-ID-TIMS dates throughout this work; Swanson-Hysell et al. (2019)). The Beaver River diabase is locally intruded by the Silver Bay intrusions (Fig. 1). An aplite unit within the granophyre zone of one of these Silver Bay intrusions has a $^{206}\text{Pb}/^{238}\text{U}$ date of 1091.61 ± 0.14 Ma (Swanson-Hysell et al., 2019). Another arcuate, sill-like diabase body mapped as the Beaver River diabase outcrops along the eastern part of the complex (Fig. 1; Miller and Chandler (1997)). The diabase composition there is similar to that in the south and it also contains large anorthosite xenoliths with dimensions that exceed 100 meters at Carlton Peak (Fig. 1). The Beaver River diabase in the northern part of the complex, near the Houghtaling Creek area, typically forms narrow, near-vertical dikes instead of sheets in the southern and eastern regions (Fig. 1; Miller et al. (1994)). The diabase in this region only locally contains xenoliths of anorthosite.

Hundreds of anorthosite xenoliths have been recognized and mapped within the Beaver River diabase (Fig. 1). Many hill tops in the Beaver Bay Complex, such as Carlton Peak and Britton Peak, are large anorthosite blocks (which lead Lawson (1893) to erroneously conclude that they were relict Archean topography). Later work established the anorthosite blocks as xenoliths, which are now extensively documented through geologic mapping of the region (Fig. 1; Miller et al. (2001); Miller (1988); Miller and Boerboom (1989); Boerboom (2004); Boerboom and Green (2006); Boerboom et al. (2006, 2007)) and outcrop-scale exposures (Fig. 2). In the field, the anorthosites typically appear as subrounded to rounded, light-colored, translucent blocks that are in sharp contact with the hosting diabase (Fig. 2). They also occur as exposures whose contact with the diabase is covered (Fig. 2). Grout (1939) suggested that the rounded anorthosites are the result of abrasion during transportation as they were entrained by the diabase (i.e. physical weathering within a magmatic system). While the Beaver River diabase is chilled against the North Shore Volcanic Group lithologies that it intrudes, the diabase is not chilled against the margin of the anorthosite xenoliths (Morrison et al., 1983; Miller & Chandler, 1997). The lack of chilled contacts is consistent with the anorthosite being at elevated temperatures and cooling at the same time as the diabase magma (Fig. 9).

The anorthosite xenoliths are dominantly monomineralic plagioclase that has an average anorthite content of $\sim 70\%$ (Morrison et al., 1983; Doyle, 2016). Interstitial pyroxene and olivine are present in minor concentrations in the xenoliths. Within the Carl-

ton Peak anorthosite xenolith, up to 10 cm oikocrysts of olivine and pyroxene can occur. Nevertheless, the overall olivine content in the anorthosites is low. Interstitial titanomagnetite-ilmenite intergrowths that exceed 100 μm can be found with microscopy and <20 μm Fe-Ti oxide grains can be detected with scanning electron microscopy (Fig. 2). Based on textural differences Morrison et al. (1983) divided the anorthosite xenoliths into four groups: one group which typically have well-developed granoblastic texture characterized by equigranular plagioclase crystals; another group which have interlocking, lath-shaped plagioclase crystals; an intermediate group which can have both granoblastic texture and interlocking plagioclase laths; and a brecciated group that have brittle deformation textures superposed on pre-existing textures.

2.2 Portage Lake Volcanics and the Greenstone Flow

The Portage Lake Volcanics (PLV) is a ~5 km thick, normally magnetized, dominantly olivine basalt to andesite volcanic succession that outcrops in northern Michigan (particularly along the Keweenaw Peninsula) as well as on Isle Royale (Fig. 1; Huber (1973); Cannon and Nicholson (2001); Green (1982)). The Greenstone Flow of the Portage Lake Volcanic Group has been recognized as one of the largest lava flows on earth (Figs. 1, 3). It outcrops as the main ridge along the Keweenaw Peninsula and Isle Royale (Fig. 1). The flow can be correlated between the two outcrop regions on the basis of geochemical, petrographic, and paleomagnetic similarity of the flow itself and the flows above and below (Longo, 1984). In both outcrop regions, the Greenstone Flow is underlain by conglomerate and overlain by pyroclastic breccia (Lane, 1911; Huber, 1973). On the Keweenaw Peninsula, the Greenstone Flow is exposed over 90 km with a range of thickness from ~100 meters to a maximum thickness of over 450 meters, dipping to the northwest (Fig. 1; White (1960)). On Isle Royale, the Greenstone Flow has a range of thickness from ~30 meters to a maximum thickness of about 250 meters, dipping toward the southeast (Fig. 1; Huber (1973)). More recently, Doyle (2016) estimated that the total aerial extent of the Greenstone Flow could be up to ~20000 km^2 by connecting it to the region of the Beaver Bay Complex. Taking thickness range of 100 to 300 meters, Doyle (2016) estimated a total volume of 2000 to 6000 km^3 . This volume range makes the Greenstone Flow one of the largest, if not the largest, single mafic lava ows on Earth (Fig. 3).

According to the mineralogical and textural attributes, the Greenstone Flow can be divided into four zones from bottom to top — a lower ophitic zone, a “pegmatoid”

or heterolithic zone, an upper ophitic zone, and an amygdaloidal zone (Cornwall, 1951). The heterolithic zone contains lenses to layers of coarse-grained granophyric gabbro that are referred to in the literature as “pegmatoid.” Zircon crystallized in these layers have enabled the heterolithic zone to be targeted for U-Pb geochronology (Davis & Paces, 1990; Swanson-Hysell et al., 2019). A $^{206}\text{Pb}/^{238}\text{U}$ zircon date of 1091.59 ± 0.27 Ma for the Greenstone Flow was developed from a sample from this zone in Swanson-Hysell et al. (2019). The Greenstone Flow is typically interpreted to represent emplacement of a single body of magma that then underwent in situ differentiation (Huber, 1973; Davis & Paces, 1990). Doyle2016a favored a distinct model in which the Greenstone Flow is a composite unit, which they interpret to be indicated by lithologic zonation of ophitic basalt forming the upper and lower zones and an interior zone composed of prismatic ferrogabbro to granophyric monzodiorite. They envision emplacement of the Greenstone Flow started with voluminous eruption of olivine tholeiitic magma, forming the ophitic zones which while still crystallizing further inflated due to subsequent injection of a more evolved basaltic magma to form intergranular gabbro in the heterolithic zone. They considered this progression to be more consistent with observed abrupt lithologic changes from the ophitic zone to the heterolithic zone over centimeter to meter scales, inclusion relationships between evolved and ophitic Greenstone Flow lithologies, and remnant blocks of initially crystallized ophitic basalt interlayered with evolved lithologies within the heterolithic zone which contains the pegmatoids. In both the Doyle (2016) model of multiple magma injections and the earlier models of in situ differentiation, it is migration of the most evolved and volatile-rich melts within the interior of the flow in the final stages of flow crystallization that led to the formation of some aplite dikes and the coarsest segregations containing granophyre. Both models also invoke a single basaltic parental magma with distinction of where differentiation occurred in fractionally crystallizing an evolving magma chamber or solely within a single, very thick flow.

250 3 Methods and Results

251 3.1 Zircon Geochronology and Geochemistry

252 A sample of an anorthosite xenolith within the Beaver River diabase was collected
 253 for U-Pb geochronology along Hwy 61 across from the Silver Bay taconite plant (MS99033;
 254 91.26358°W 47.28888°N; Fig. 1). This sample comes from the same xenolith sampled for
 255 paleomagnetic study as site AX16 which has an exposed diameter of 27.5 meters (Fig.

256 2). Thin sections were made from the geochronology sample as well as multiple paleo-
257 magnetic cores. As is shown in Fig. 2F, plagioclase in this anorthosite xenolith have both
258 equigranular crystals displaying a granoblastic texture and lath-shaped crystals display-
259 ing an interlocking texture. The occurrence of both textures is consistent with an inter-
260 pretation that this anorthosite xenolith formed under elevated temperatures and expe-
261 rienced heating after initial crystallization.

262 Zircons were separated from a kilogram of the anorthosite using common mineral
263 separation methods (Supporting Information). The separated zircons were subhedral to
264 anhedral crystals (z1-z4) and platy fragments (z5-z8). The subhedral to anhedral crys-
265 tals are consistent with intercumulus crystallization within an adcumulate with platy frag-
266 ments also being a common zircon morphology within anorthosites (e.g. sample AS3 of
267 the Duluth Complex anorthositic series; Schmitz et al. (2003)). Eight chemically abraded
268 zircons were analyzed by isotope dilution-thermal ionization mass spectrometry (ID-TIMS)
269 in the Boise State Isotope Geology Laboratory using EARTHTIME tracer solutions (Condon
270 et al., 2015). Both zircon morphologies yield indistinguishable dates. Using six of these
271 single grain dates (and excluding two due to interpreted Pb-loss) results in a weighted
272 mean $^{206}\text{Pb}/^{238}\text{U}$ date of $1091.83 \pm 0.21/0.37/1.15$ Ma (analytical/ analytical+tracer/
273 analytical+tracer+decay uncertainty; Fig. 4).

274 This date provides a tight constraint on the age of the Beaver River diabase. Pre-
275 viously, the maximum age constraint for the Beaver River diabase came from the rela-
276 tionship that it cross-cuts the Palisade rhyolite of the North Shore Volcanic Group which
277 has a $^{206}\text{Pb}/^{238}\text{U}$ date of 1093.94 ± 0.28 Ma (Swanson-Hysell et al., 2019). With this
278 new date, we know the crystallization age of the diabase to have been near-synchronous
279 or younger than the date from the anorthosite xenolith. The Silver Bay intrusions, from
280 which an aplite has a $^{206}\text{Pb}/^{238}\text{U}$ date of 1091.61 ± 0.14 Ma, (Fairchild et al., 2017), cross-
281 cut the Beaver River diabase. These dates constrain the diabase to have been emplaced
282 between 1091.83 ± 0.21 and 1091.61 ± 0.14 Ma (Fig. 4). Assuming a uniform proba-
283 bility of diabase emplacement between the anorthosite and aplite dates and their nor-
284 mal distributed uncertainties, a 95% confidence interval on the age of the diabase can
285 be estimated by Monte Carlo simulation. This analysis gives an age for the diabase of
286 1091.7 ± 0.2 Ma (95% CI).

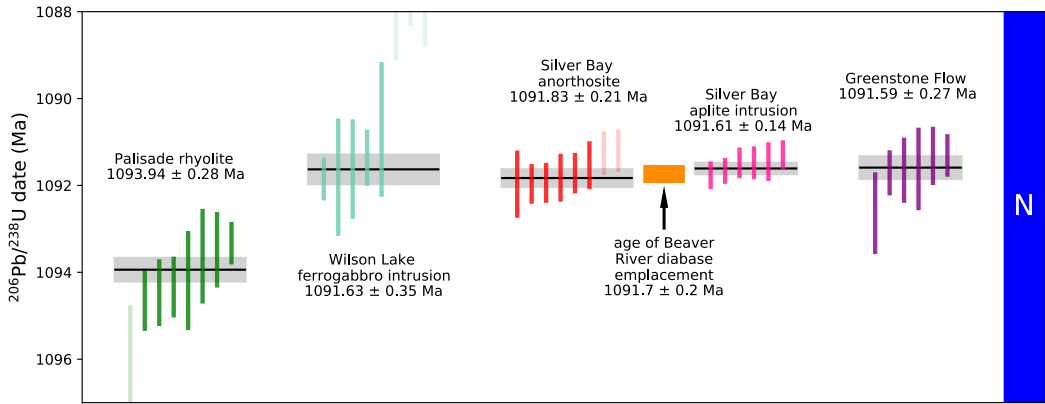


Figure 4: New $^{206}\text{Pb}/^{238}\text{U}$ zircon date of the anorthosite xenolith (dark orange) plotted in context of previously published $^{206}\text{Pb}/^{238}\text{U}$ zircon dates from the North Shore Volcanic Group (NSVG) and other Beaver Bay Complex intrusions (Swanson-Hysell et al., 2019, 2020). These high-precision dates are consistent with field observations that the Beaver River diabase crosscuts the Palisade rhyolite (dark green) and is cut by the Silver Bay intrusions (pink). The estimated age of the Beaver River diabase from these constraints is shown by an orange box representing the 95% confidence interval. Each vertical bar corresponds to one $^{206}\text{Pb}/^{238}\text{U}$ date from a single zircon crystal. The translucent bars represent zircons with interpreted Pb loss and are therefore not included in the weighted mean age calculations. Horizontal lines and gray boxes represent weighted mean $^{206}\text{Pb}/^{238}\text{U}$ dates and their analytical uncertainty. The numbers of each geochronology sample correspond to those in Fig. 1 where locations of these samples are shown.

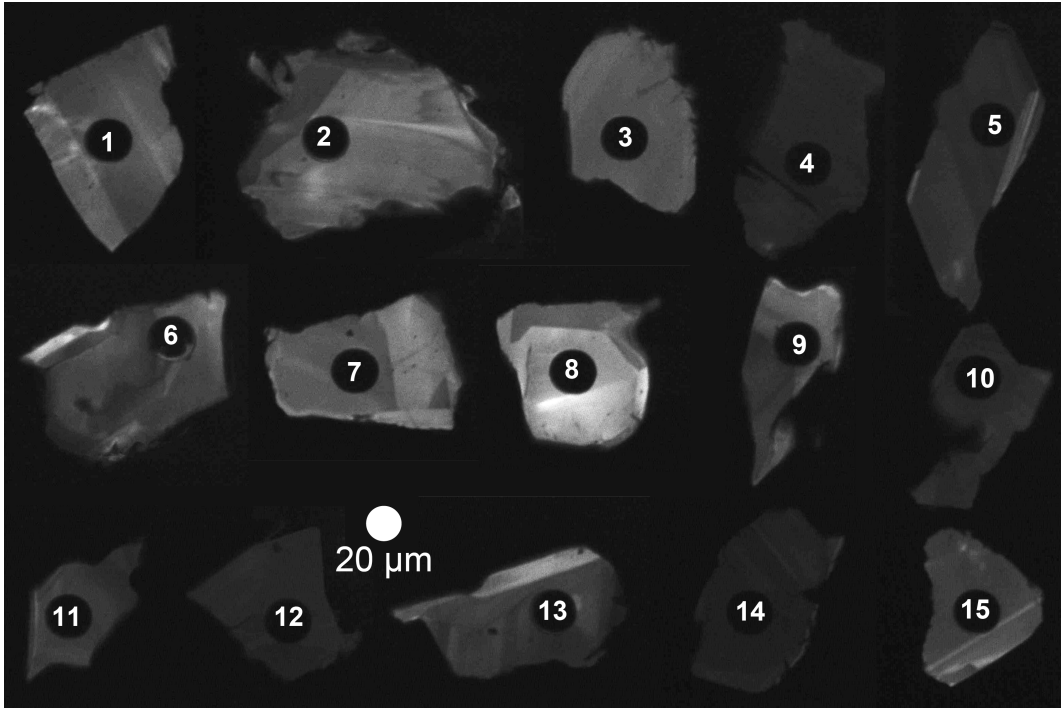


Figure 5: Cathodoluminescence (CL) image montage of the 15 zircons laser-ablated for trace element analysis from sample MS99033. There are sharp boundaries between zones of differing CL response within many of the zircons attributable to variable REE concentrations. For example, the bright zoning in grain 15 has a thickness of $\sim 2 \mu\text{m}$. Note that grain 1 (corresponding to spot 1) has a platy morphology, while the rest of the grains are subhedral to anhedral.

An additional 15 zircons were characterized using cathodoluminescence (CL) imaging and laser ablation-inductively coupled plasma mass spectrometry (LA-ICPMS), with methods and instrumentation described in the Supporting Information. CL images reveal internal planar zones of variable brightness, often with darker interior zones and outer brighter zones (Fig. 5). All crystals exhibit sharp, micron-scale transitions between zones, and LA-ICPMS analyses quantify CL brightness as correlated with rare earth elements (REE) content. REE patterns in zircons exhibit a significant chondrite-normalized negative Eu anomaly (Fig. 6). The Ti-in-zircon thermometer gives a range of estimated zircon crystallization temperatures from 998°C to 860°C with a mean of $\sim 950^\circ\text{C}$ (Ferry and Watson (2007); Supporting Information). Decreasing temperatures are correlated with deepening of the negative Eu anomaly and increasing incompatible trace element (e.g. Hf, Th) incorporation into zircon. These data are consistent with a model of magmatic

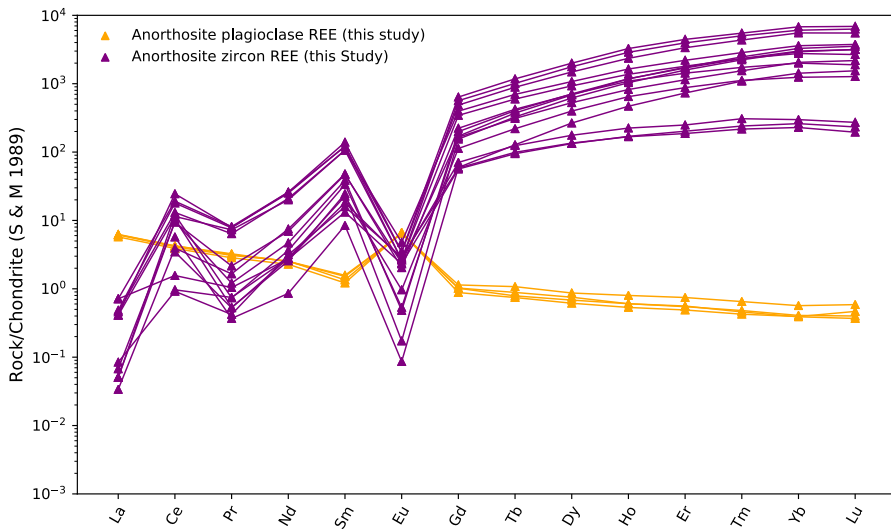


Figure 6: Rare earth element (REE) analyses for 4 plagioclase crystals and for 15 zircons from geochronology sample MS99033 (anorthosite xenolith site AX16) developed by inductively coupled plasma mass spectrometry. All data are chondrite-normalized (Sun & McDonough, 1989).

299 zircon crystallizing from cooling and fractionating interstitial residual melt within the
300 cumulate plagioclase framework.

301 3.2 Paleomagnetism

302 We collected paleomagnetic cores that are 2.5 cm in diameter along the southern
303 and eastern Beaver Bay Complex with a particular focus on acquiring paired sites of anorthosite
304 xenoliths and their local diabase hosts. Sample cores were collected using a hand-held
305 gasoline-powered drill and were oriented using a magnetic compass as well as a sun com-
306 pass when possible. Sun compass orientations were preferentially used for determining
307 the sample azimuth. Typically, 7-10 cores were collected for each anorthosite xenolith
308 and their diabase hosts. A total of 17 diabase and 22 anorthosite sites were sampled (Ta-
309 ble 1). A table that summarizes the measured dimensions of each anorthosite xenolith
310 sampled and the distance between each anorthosite paleomagnetic site and closest di-
311 abase host site is provided in the Supporting Information.

Samples underwent step-wise demagnetization and analyses in the magnetically-shielded room at the UC Berkeley Paleomagnetism Lab. 7 sites from the Beaver River diabase underwent alternating field (AF) demagnetization with peak fields from 1 mT to 130 mT. An ASC TD-48SC thermal demagnetizer was used to demagnetize 10 diabase sites and all 22 anorthosite sites in a step-wise manner, with reduced step increments between 540°C and 585°C. The typical magnetic field inside the shielded room is <500 nT and the field inside the thermal demagnetizer chamber is <10 nT. The quartz glass sample rod of the UC Berkeley system is typically measured at 5×10^{-12} Am². All remanence measurements were made on a 2G Enterprises DC-SQUID superconducting rock magnetometer equipped with inline AF coils and an automated sample changer system. The PmagPy software package was used to implement least-square fits to specimen demagnetization data (Tauxe et al., 2016). Measurement level data are available within the MagIC database (<https://earthref.org/MagIC/17102/400e0fb3-a79b-42bd-aeab-9005d2e3b438>; UPDATE ONCE PUBLICATION DOI IS GENERATED)

For both the diabase and anorthosite demagnetization, principal component analyses show that an origin trending characteristic remanent magnetization (ChRM) can be isolated after the removal of a minimal secondary component during the first few low coercivity (<10 mT) or low temperature (<200°C) demagnetization steps (Fig. 7). The ChRMs typically unblock through thermal demagnetization steps from ~500°C to ~580°C, consistent with the component being held by low-titanium titanomagnetite. We interpret this component as a primary remanent magnetization acquired during the emplacement and cooling of the Beaver River diabase.

The site mean paleomagnetic directions are shown in Table 1. We present both AF and thermal demagnetization results for the Beaver River diabase as both methods are effective in removing the secondary components and isolating the coherent and univectoral ChRM. Based on specimen and site level demagnetization behavior and the proximity between paired paleomagnetic sites of the anorthosite xenoliths and the diabase, we grouped the anorthosite xenoliths and their diabase hosts into individual cooling units and calculated a paleomagnetic pole position from the mean of the cooling unit virtual geomagnetic poles (Fig. 8).

Tilt-correcting the paleomagnetic directions to paleohorizontal is necessary for developing accurate paleomagnetic poles from the diabase and the anorthosite xenoliths

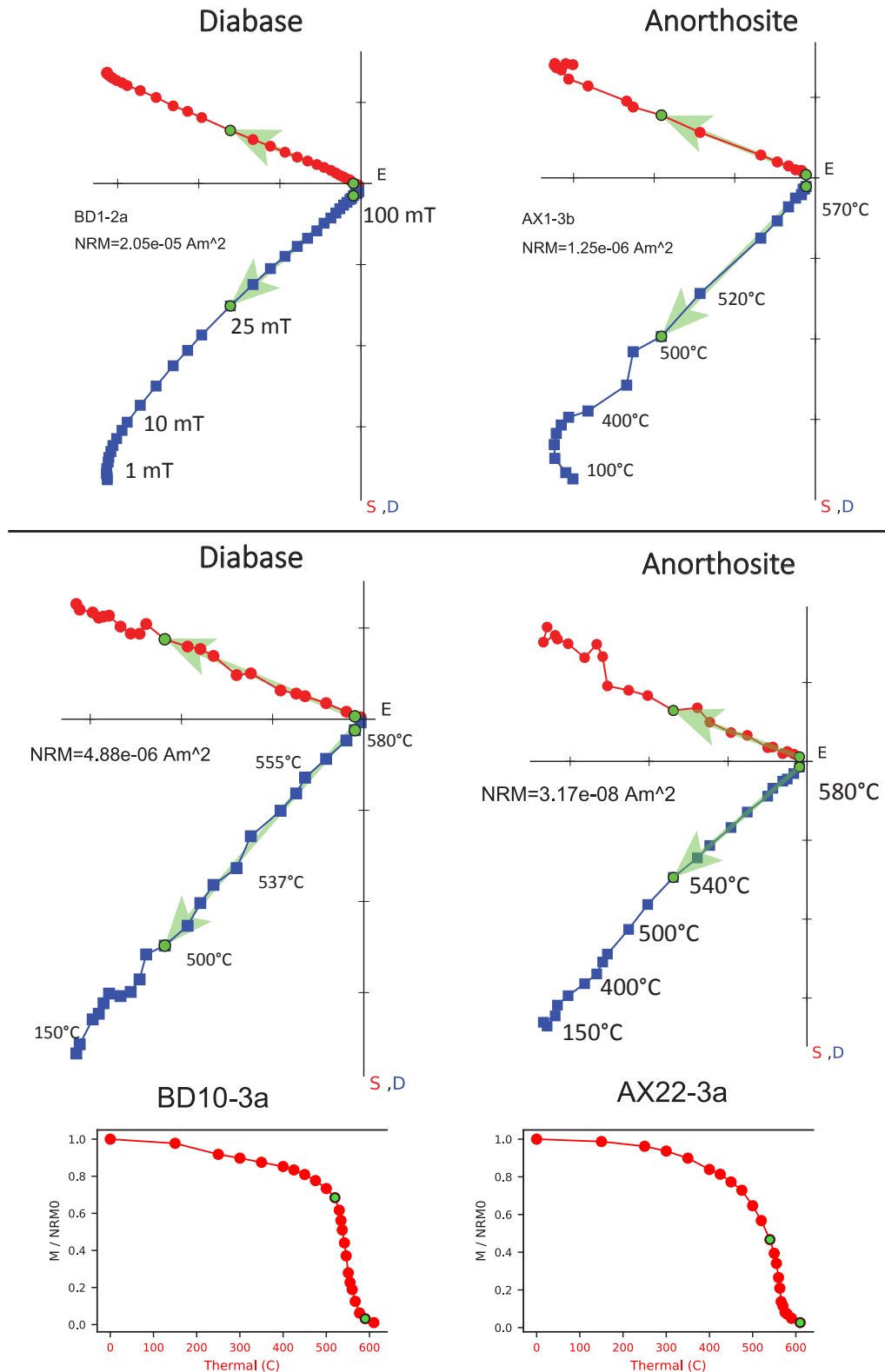


Figure 7: Example orthogonal vector demagnetization diagrams for diabase and anorthositic xenoliths. Anorthosite site AX1 is a xenolith within the diabase sampled as BD1. Similarly, AX22 is from a xenolith within the BD10 diabase. Both AF and thermal demagnetization show dominantly univectoral decay of characteristic remanent magnetizations (ChRM) toward the origin after removal of minimal secondary components. The data show very similar ChRM directions between the paired diabase and anorthositic xenoliths sites. Representative magnetization intensity versus thermal demagnetization step plots are paired with orthogonal vector plots for specimen BD10-3a and AX22-3a.

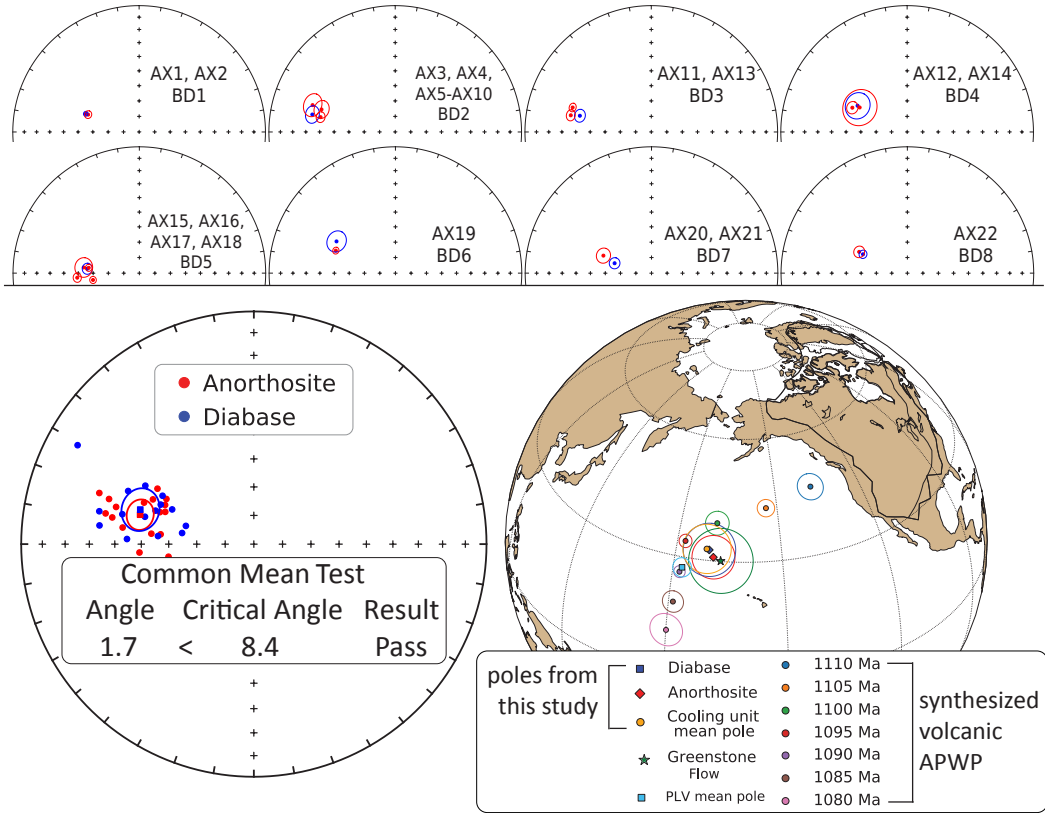


Figure 8: Top: Equal area plots of paleomagnetic directions from the anorthosite xenoliths and their local diabase hosts. AX: anorthosite xenolith site; BD: Beaver River diabase site. Bottom: Site mean paleomagnetic directions from the Beaver River diabase and anorthosite xenoliths are plotted on equal area plots. The anorthosite and diabase sites share a common mean as summarized by the results of the McFadden and McElhinny (1990) common mean test. Mean paleomagnetic pole positions of all diabase sites, all anorthosite sites, as well as a grand mean pole developed by grouping the anorthosite and diabase sites into individual cooling units are plotted against a synthesized Laurentia APWP based on poles from Midcontinent Rift volcanics and sedimentary rocks (Swanson-Hysell et al., 2019). The paleomagnetic poles from the diabase and anorthosite are indistinguishable with the Greenstone Flow pole developed by Foucher (2018), but they all are distinct from the Portage Lake Volcanics mean pole (Swanson-Hysell et al., 2019). All directions shown are tilt corrected.

344 to be compared to the Keweenawan Track apparent polar wander path (APWP; Fig. 8,
 345 Swanson-Hysell et al. (2019)). For intrusive igneous rocks, tilt corrections can be diffi-
 346 cult to constrain due to the lack of a clear paleohorizontal reference. Many paleomag-
 347 netic studies of Midcontinent Rift intrusive rocks in the Lake Superior region did not ap-
 348 ply tilt corrections to their data (e.g., Beck & Lindsley, 1969; Beck, 1970; Books et al.,
 349 1966). However, we can determine the structural orientation of the Beaver River diabase
 350 using the abundant igneous fabric orientations measured on the diabase as well as bed-
 351 ding orientations measured from adjacent volcanic units (Boerboom, 2004; Boerboom
 352 & Green, 2006; Boerboom et al., 2006, 2007; Miller et al., 2001). We compile the igneous
 353 layering measurements from the Beaver River diabase and the volcanic bedding ori-
 354 entations from the Schroeder-Lutsen basalt which is overlying the Beaver Bay Complex
 355 (Fig. 1). Despite the uncertainties associated with using igneous fabrics orientations as
 356 paleohorizontal references, the mean tilt orientations of the fabrics of the Beaver River
 357 diabase and the volcanic bedding orientations of the Schroeder-Lutsen basalt are sim-
 358 ilar (diabase overall dip direction - dip: 128.5 - 10.2; basalt dip direction - dip: 142.2 -
 359 13.6). We combine the structural measurements from the Beaver River diabase and the
 360 Schroeder-Lutsen basalt and derived two sets of tilt corrections for the paleomagnetic
 361 directions of the diabase and anorthosite (dip direction - dip in the southern Beaver Bay
 362 complex: 128.7 - 12.9; in the eastern Beaver Bay Complex: 145.6-13.1, Supporting In-
 363 formation). The advantage of using the structural orientations from the Schroeder-Lutsen
 364 basalt is that the arcuate shape of the Beaver River diabase intrusions is nicely captured
 365 by the variation of lava dip directions while the dip angles of the basalt and diabase are
 366 very similar (Fig. 1).

367 The tilt-corrected ChRMs in both lithologies are west-northwest and down, yield-
 368 ing good specimen-level and site-level consistency (Figs. 7 and 8). Close directional sim-
 369 ilarities between each anorthosite xenolith and their host diabase are supported by 9 out
 370 of a total of 17 diabase-anorthosite paleomagnetic site pairs passing a common mean test
 371 (McFadden & McElhinny, 1990). The overall mean directions between the two litholo-
 372 gies are indistinguishable as they also pass a common mean test (Fig. 8, McFadden and
 373 McElhinny (1990)). For the anorthosite sites that do not pass a common mean test with
 374 their diabase hosts, they nevertheless have coherent specimen-level directions that are
 375 close to their host diabase directions (Fig. 8). We also plot the tilt-corrected mean pole
 376 of sites from both lithologies (diabase: 32.5°N, 189.5°E, N = 15, A95 = 6.3, k = 37.4;

377 anorthosite: 30.9°N, 190.8°E, N = 17, A95: 5.2, k = 48.5; Table. 1) in context of a pre-
 378 previously synthesized APWP from the volcanics of the Midcontinent Rift (Swanson-Hysell
 379 et al., 2019) and show the poles to lie near the expected 1090 Ma and 1095 Ma pole po-
 380 sitions (Fig. 8). The mean pole position of the interpreted cooling units (32.7°N, 188.8°E,
 381 N = 15, A95 = 5.9, k = 41) lies close to the mean pole position derived from the *ca.* 1092
 382 Ma Portage Lake Volcanics (Fig. 8), consistent with the coeval magmatic activity be-
 383 tween the Beaver River diabase and the Portage Lake Volcanics. If it is included in fu-
 384 ture Laurentia APWP compilations, it is this cooling unit mean pole paired with the es-
 385 timated diabase emplacement age of 1091.7 ± 0.2 Ma that should be used.

386 3.3 Thermal history model

387 The consistency of the paleomagnetic directions between the anorthosite xenoliths
 388 and the host diabase indicate that the anorthosites were heated above the Curie tem-
 389 perature of low-titanium titanomagnetite ($\sim 580^\circ\text{C}$) within the Beaver River diabase. To
 390 determine whether this thermal history is consistent with the geometry of the units and
 391 to gain more insight into the emplacement history of the xenoliths, we developed a cool-
 392 ing model. In this model, the anorthosite xenoliths are considered to be solid spheres
 393 with an initial cool temperature embedded in a uniform sheet of diabase magma (Delaney,
 394 1987; Unsworth & Duarte, 1979). The modeled thermal histories for various sizes of anorthosite
 395 xenoliths are shown in Fig. 9. In one end member case, the initial temperature of the
 396 anorthosites is assumed to be 50°C . While this temperature is unrealistically low given
 397 that the anorthosites likely have a deep crustal source, thermal modeling shows that even
 398 a 100-meter anorthosite xenolith with such low initial temperature would have been heated
 399 to the temperature of the tholeiitic magma (1150°C) within the sill. This temperature
 400 is well above the Curie temperature of magnetite. Anorthosite xenoliths with an assumed
 401 initial temperature of 500°C will equilibrate with the magma temperature on a similar,
 402 but slightly shorter, timescale. Therefore, the model predicts that the remanent mag-
 403 netizations of the anorthosites will be reset during emplacement within the diabase sills,
 404 regardless of their initial temperatures. Model parameters set to match the xenolith AX16,
 405 from which a U-Pb date was developed in this study, leads to a model where the 27.5
 406 m xenolith would have stayed at the magma temperature for about 100 years after sill
 407 emplacement (Fig. 9). This duration estimate is a minimum as it does not consider heat-
 408 ing associated with melt in the lower crust or during ascent prior to emplacement although

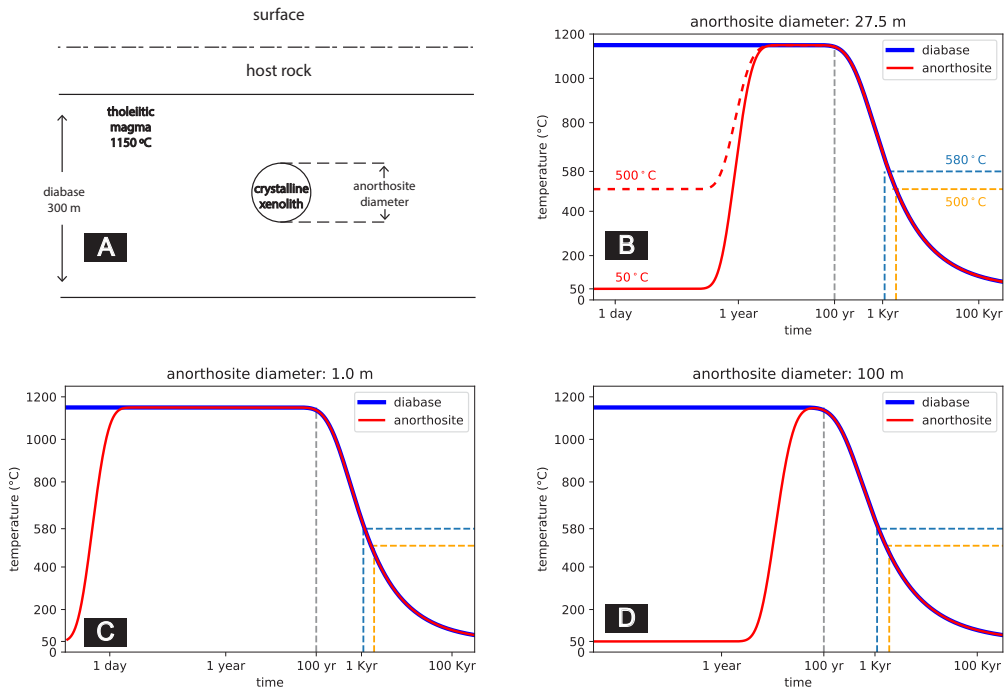


Figure 9: Thermal history model of the Beaver River diabase and its anorthosite xenoliths after emplacement at hypabyssal depths. (A) Schematic diagram for the thermal model considering cool anorthosite xenoliths as crystalline spheres residing in the middle of a diabase sill. Together they are hosted by cool country rocks at shallow depths. (B) Specific model for anorthosite AX16 (diameter of 27.5 meters) within its diabase sill host which is estimated to be 323 meters thick. (C) Thermal history model considering an anorthosite xenolith 1 meter in diameter residing in a 300 meter diabase sill. (D) Thermal history model considering an anorthosite xenolith 100 meter in diameter residing in a 300 meter diabase sill. These models show that anorthosite xenoliths were heated up to the diabase melt temperature after the emplacement, regardless of size. The time elapsed between at magnetite blocking temperatures (580°C and 500°C) during cooling is on the scale of a thousand years.

409 this was likely rapid. The xenolith would have then cooled through the Curie temper-
 410 ature of magnetite (580°) after ~ 1 kyr and acquired its magnetization as it cooled through
 411 magnetite blocking temperatures (down to $\sim 500^{\circ}$, Fig 7).

412 4 Discussion

413 4.1 Origin and Age of the Anorthosite Xenoliths

414 There have been divergent interpretations regarding the age and magma source of
 415 the anorthosite xenoliths in the Beaver River diabase (Fig. 1). Grout (1939) recognized
 416 the xenolithic nature of the anorthosites and suggested that the massive intrusion of the
 417 older anorthositic gabbro within the Duluth Complex may have supplied anorthosite frag-
 418 ments that were later entrained by the Beaver River diabase emplacement. Morrison et
 419 al. (1983), on the other hand, argued that the xenoliths were sourced from Paleoprotero-
 420 zoic or Archean lower crust that were liberated and contaminated by Midcontinent Rift
 421 magmas based on Sm and Nd isotopic data. They interpreted a Sm-Nd model age of 1.9
 422 Ga from one of the xenoliths as providing a minimum crystallization age for the anorthosites
 423 though they acknowledged that these constraints are not definitive with respect to the
 424 age.

425 In contrast to this Archean to Paleoproterozoic model, Miller and Chandler (1997)
 426 favored a scenario where the anorthosite crystallized as part of Midcontinent Rift mag-
 427 matism. They cited work by Kushiro (1980) who showed that the changing density con-
 428 trast between labradoritic to bytownitic plagioclase and tholeiitic magma at different crustal
 429 pressures would promote flotation of plagioclase in deep (>20 km) crustal magma cham-
 430 bers and the creation of anorthosite cumulates in the lower crust. This mechanism of
 431 plagioclase flotation likely created massive anorthosite cumulates in the roof zones of sub-
 432 crustal magma chambers during MCR magmatism. Miller and Weiblen (1990) specu-
 433 lated that plagioclase-phyric magmas tapped from these deep chambers fed shallow (~ 5
 434 km) subvolcanic intrusions of the Duluth Complex, thereby creating the troctolitic anorthosites
 435 and gabbroic anorthosites of the Anorthositic Series. Miller and Chandler (1997) sug-
 436 gested that the nearly pure anorthosite xenoliths occurring in the younger and more hy-
 437 pabyssal diabase intrusions of the Beaver Bay Complex were harvested from these phase-
 438 segregated intrusions in the lower crust. They further argued that the isotopic data of
 439 Morrison et al. (1983) can be explained by anorthosite-forming MCR magmas having

440 been contaminated by older crust rather than the anorthosites being older lower crust
 441 that was contaminated by MCR magmas.

442 Our new geochronology documents that the anorthosite xenoliths were liberated
 443 from depth and were emplaced within the shallow intrusions of the Beaver River diabase
 444 at 1091.7 ± 0.2 Ma (95% CI). This timing of emplacement is constrained by the Beaver
 445 River diabase postdating the new $^{206}\text{Pb}/^{238}\text{U}$ zircon date of 1091.83 ± 0.21 Ma for the
 446 AX16 xenolith and being older than the cross-cutting 1091.61 ± 0.14 Ma Silver Bay in-
 447 trusives.

448 The most straight-forward interpretation of the anorthosite 1091.83 ± 0.21 Ma U-
 449 Pb zircon dates is that they record crystallization of the anorthosite cumulates during
 450 Beaver Bay Complex magmatism just before the time of Beaver River diabase emplace-
 451 ment. The significant negative Eu anomaly in the zircons within the anorthosite con-
 452 strains them to have crystallized from a magma that had experienced significant plagi-
 453oclase extraction (Fig. 6; Rubatto (2002); Schaltegger et al. (1999)). This result indicates
 454 that the zircons were comagmatic with their host anorthosite plagioclase. The Ti-in-zircon
 455 temperature estimates indicate that they crystallized from temperatures of ~ 998 to 860°C
 456 (Supporting Information; Ferry and Watson (2007)). In addition, zircons that have lower
 457 Ti-in-zircon temperatures have lower Eu abundance, but enrichment of incompatible el-
 458 ements such as Hf and Th (Supporting Information). This systematic pattern of elemen-
 459 tal concentration variation is consistent with the zircons crystallizing from residual melts
 460 on a cooling path that increased incorporation of incompatible trace elements and deep-
 461 ened the Eu anomaly with decreasing temperature and melt fraction. Scanning electron
 462 microscopy on two undated anorthosite xenoliths with plagioclase laths displaying in-
 463 terlocking textures shows zircon crystals with subhedral to anhedral shapes within the
 464 mineral assemblage that is interstitial to the plagioclase (Supporting Information). Cathodo-
 465 luminescence (CL) images show internal zoning in zircons which can be attributed to vari-
 466 ations in REE, particularly Dy elemental concentrations, during zircon crystallization
 467 (Fig. 5; Remond et al. (1992)). These data confirm that the zircons formed from resid-
 468 ual melt within the interstitial spaces of the plagioclase cumulate and are inconsistent
 469 with a later metamorphic origin.

470 This scenario requires that there were large lower crustal magma chambers in which
 471 flotation of plagioclase resulted in cumulate formation during *ca.* 1092 Ma Beaver Bay

472 Complex magmatism and contrasts with the model of Miller and Chandler (1997) for
473 an older origin of the anorthosite during the *ca.* 1096 Ma Duluth Complex magmatism.
474 Zircon U-Pb dates nearly always record crystallization age as the temperatures neces-
475 sary for significant diffusive Pb loss exceed typical liquidus temperatures of zircon-bearing
476 rocks. However, the anorthosites are a rather unique case given that the melting point
477 of anhydrous plagioclase with an average composition of the Beaver River anorthosite
478 (\sim 70% anorthite, Morrison et al. (1983); Doyle (2016)) is quite high at \sim 1400°C. Ther-
479 mal modeling indicates that the xenoliths would have equilibrated to the temperature
480 of the olivine tholeiitic magma (\sim 1100 to 1200°C) and remained at that temperature for
481 more than 100 years in the diabase sill interior (Fig. 9). While these temperatures would
482 not have melted the plagioclase or zircon, these temperatures are high enough to con-
483 sider the possibility of Pb diffusion out of zircon. Could diffusive resetting of the zircon
484 in the anorthosite cumulates xenoliths allow their crystallization at *ca.* 1096 Ma in the
485 deep crust, but the closure of U-Pb zircon chronometer upon emplacement and cooling
486 at *ca.* 1091.8 Ma?

487 The magnitude of Pb diffusion is dependent on the time spent at such a temper-
488 ature. Using the diffusion parameters of Cherniak and Watson (2001), a sustained tem-
489 perature of 1200°C for \sim 10 thousand years is required for diffusive loss of \sim 90% of Pb
490 from a \sim 120 μm diameter zircon. In this case, zircons that crystallized at 1096 Ma and
491 then lost $>90\%$ of their Pb at 1091.6 Ma could give apparent U-Pb dates of 1091.8 Ma
492 that are reproducible at the measurement resolution (Fig. 10). However, CL imagery
493 reveals sharp boundaries between zones of differing CL response (Fig. 5) on the scale
494 of \sim 2 μm . Such CL zoning patterns are dominantly attributed to concentration varia-
495 tions in the rare earth element Dy (Remond et al., 1992). A time-temperature history
496 that results in 90% Pb diffusion out of a 120 μm diameter zircon would also cause Dy
497 re-equilibration throughout a zircon, leaving no clear zonation (Fig. 10; Cherniak et al.
498 (1997)). Therefore, a scenario where the zircons first crystallized during Duluth Com-
499 plex magmatism and subsequently lost more than 90% of Pb is exceedingly difficult to
500 reconcile with the preservation of such thin, sharp zones. In fact, preservation of REE
501 zoning in these zircons limits heating at the emplacement temperatures of the Beaver
502 River diabase to a duration more consistent with our modeled duration of \sim 100 years
503 of heating prior to cooling to the temperatures that preserve such zonation (Fig. 9, 10).

504 It is therefore most probable that the Beaver River diabase anorthosite xenoliths are en-
 505 trained cumulate enclaves that formed at the time of Beaver Bay Complex magmatism.

506 **4.2 A comagmatic relationship between the Beaver River diabase and
 507 the Greenstone Flow**

508 Given the existence of many anorthosite xenoliths whose short-axis diameters of-
 509 ten reach tens of meters and can be as wide as 180 meters (Fig. 1; Boerboom (2004);
 510 Boerboom et al. (2006)), the Beaver River diabase magma conduits must have been at
 511 least this wide during magma ascent. It would be consistent with such wide conduits ex-
 512 tending to hypabyssal depths for magma that flowed through these conduits to have vented
 513 to the surface.

514 The high volume of the extrusive Greenstone Flow of the Portage Lake Volcanics
 515 lead to a potential match for this large feeder system. Doyle (2016) proposed a comag-
 516 matic link between the Beaver River diabase and the Greenstone Flow. Doyle (2016) dis-
 517 covered that both the intrusive Beaver River diabase and the Greenstone Flow have in-
 518 distinguishable primary compositions that followed similar differentiation patterns. Doyle
 519 (2016) also highlighted the shared petrographic textures between the ophitic Beaver River
 520 diabase and the ophitic Greenstone Flow, which features the plagioclase laths cluster-
 521 ing together and joining along their long crystallographic axes. The fosterite content of
 522 the olivines and enstatite content of the pyroxenes in the Beaver River diabase together
 523 with the Silver Bay intrusions, and the Greenstone Flow have overlapping compositions
 524 consistent with the same magma source (Fig. 11). The composition of the plagioclase
 525 within the units further strengthens this interpretation. Although there are no known
 526 multi-crystalline anorthosite xenoliths in the Greenstone Flow, plagioclase megacrysts
 527 occur in the lava flow. Analyses of the anorthite content from plagioclase megacrysts show
 528 very similar values between the Beaver River diabase and the Greenstone Flow basalt
 529 (Fig. 11; Doyle (2016)). In both units, the plagioclase cores are more enriched in anor-
 530 thite than the rim and the groundmass. These data provide evidence that the core of
 531 the plagioclase megacrysts in the Greenstone Flow derived from a similar source with
 532 those in the Beaver River diabase and that the rims are later overgrowths. These min-
 533 eralogical similarities are consistent with the interpretation that the Beaver River dia-
 534 base and the Greenstone Flow have the same magma source.

The synchronicity between the Beaver River diabase and the Greenstone Flow inferred from comparable lithologies and geochemistry can be further evaluated using the paleomagnetic pole positions and radioisotopic dates from both units (Fig. 8, 4). The heat diffusion model of the cooling history of the anorthosite xenoliths within the diabase suggests that the time it takes to cool the diabase and anorthosite from low-titanium titanomagnetite Curie temperature ($\sim 580^{\circ}\text{C}$) to their blocking temperatures ($\sim 500^{\circ}\text{C}$) is on the time scale of a few thousand years (Fig. 9). This time scale is close to the typical 10^4 years which is considered to be sufficient for averaging out secular variations of the geomagnetic field. Fig. 8 shows the site mean paleomagnetic pole positions from all diabase and anorthosite sites in this study against the previously synthesized Laurentia APWP developed using an Euler pole inversion to chronostratigraphically constrained volcanic poles in present-day coordinates (Swanson-Hysell et al., 2019). The site-mean pole positions of the diabase and anorthosite overlap within uncertainty ellipses and the mean pole positions fall between the 1095 Ma and 1090 Ma pole path positions (Fig. 8), consistent with the geochronology results (Fig. 4). Further, the mean paleomagnetic pole position derived from the Greenstone Flow share a common mean with those of the Beaver River diabase and the anorthosite xenoliths, but these poles do not share a common mean with the mean pole derived from the Portage Lake Volcanics (Fig. 8; Swanson-Hysell et al. (2019)). This result suggests that the timescale over which the Beaver River diabase and the Greenstone Flow acquired their magnetization may be too short to fully average out secular variation. In this case, the overlapping pole positions between the Beaver River diabase and the Greenstone Flow strengthens their temporal correlation even more (Fig. 8).

The U-Pb dates are consistent with a comagmatic relationship as they reveal indistinguishable ages for the Beaver River diabase and the Greenstone Flow. The age of the Beaver River diabase is constrained to be between the $^{206}\text{Pb}/^{238}\text{U}$ dates of 1091.83 ± 0.21 Ma and 1091.61 ± 0.14 Ma (Fig. 4) giving an age estimate of 1091.7 ± 0.2 Ma (95% CI). This age is indistinguishable with the $^{206}\text{Pb}/^{238}\text{U}$ date of 1091.59 ± 0.27 Ma for the Greenstone Flow (Fig. 4).

The Portage Lake Volcanics, including the Greenstone Flow, are interpreted to have erupted into the main central graben of the Midcontinent Rift during an interval of significant subsidence (Fig. 12; Miller and Chandler (1997); Cannon and Hinze (1992)). In contrast to the thick accumulation in the Portage Lake Volcanics, the Beaver Bay Com-

plex has an erosional (and slightly angular) unconformity atop it that is then covered by the younger Schroeder-Lutsen basalt (Fig. 1; Miller et al. (2001)). This relationship suggests that the Beaver River diabase was emplaced into a rift flank highland that experienced uplift during the active development of the central graben (Swanson-Hysell et al., 2019). Eruptions fed through the Beaver River diabase network would have emerged from the rift flank and flowed from the highland into main rift basin (Fig. 12).

The proposed intrusive-extrusive connection between the Beaver River diabase and the Greenstone Flow would imply that the Greenstone Flow extended for more than 250 km from northeastern Minnesota to the northern end of Isle Royale where the flow is ~100 m thick and to the northeastern end of the Keweenaw Peninsula, where the flow is ~400 m thick (Fig. 1). With this length, the full volume of the Greenstone Flow reaches ~6000 km³ (Doyle, 2016), rivaling the largest known lava flows on Earth (Fig. 3). Such lengths were achieved for multiple high volume flows within the Columbia River basalts (Reidel et al., 2013) and are modest compared to the Rajahmundry Trap lavas of the Deccan Traps which traveled ~1000 km (Self et al., 2008). One potential challenge for a flow having traveled from the Beaver River diabase to the Portage Lake Volcanics is that a reconstruction of present-day rift basin isopachs from seismic data indicates that there is a deep bowl-shaped volcanics-filled basin offshore of Minnesota and the Beaver Bay Complex (Stewart et al., 2018). While this basin has a thicker accumulation of volcanics than surrounding regions, it is unclear whether it was a topographic barrier. If it was, it could have prevented lavas from present-day northern Minnesota from reaching the portion of the basin now exposed on the Keweenaw Peninsula. Therefore, it is also possible that the indistinguishable ages and similar geochemistry between the Beaver River diabase and the Greenstone Flow are the result of them having been derived from a contemporaneous deep magmatic source without being connected on the surface.

5 Conclusion

There was voluminous emplacement of magma into the shallow subsurface and eruption into the Midcontinent Rift basin *ca.* 1092.7 Ma at the end of the main stage of Midcontinent Rift volcanism. The anorthosite xenoliths within the Beaver River diabase and their U-Pb geochronology, whose interpretation is informed by REE patterns, indicate that there was a contemporaneous deep crustal magmatic system in which flotation of plagioclase formed anorthosite cumulates. The large dimension of the anorthosite xeno-

600 liths require that conduits feeding magma to the surface had widths that exceeded 150
601 meters. These conduits would have delivered a high volume of magma into the rift basin.
602 The high-precision U-Pb dates, together with paleomagnetic and geochemical data, are
603 consistent with the hypothesis that the Beaver River diabase was the feeder system of
604 the Greenstone Flow although they could have been disconnected at the surface and both
605 be emblematic of this high-volume pulse of magmatism..

606 **Acknowledgments**

607 Project research was supported by NSF CAREER grant EAR-1847277 to N.L.S.-H. and
608 an Institute on Lake Superior Geology Student Research Fund grant to Y.Z. Permits for
609 fieldwork and sampling from the Minnesota Department of Natural Resources are grate-
610 fully acknowledged. We thank James Pierce and Blake Hodgin for assistance in the field.
611 We thank Stephen Self for providing constructive comments regarding mafic lava flow
612 volumes. We thank John Grimsich and Tim Teague at UC Berkeley EPS department
613 for their help with petrographic sample preparation and analyses. We thank U.S. Ge-
614 ological Survey reviewer Jonathan Hagstrum and journal reviewers Bernie Housen and
615 William Rose for their constructive comments on the manuscript. Paleomagnetic data
616 associated with this study are available within the MagIC database (<https://earthref.org/MagIC/17089/26d9073f-2447-4f46-85fb-8596ce5b3aab>; UPDATE WHEN DOI
617 IS GENERATED) and all data are within a Github repository associated with this work
618 (https://github.com/Swanson-Hysell-Group/2021_AX_BD) that is also archived on Zen-
619 odo (<https://doi.org/10.5281/zenodo.5394529>). This repository also contains Python
620 code related to calculations, visualizations and statistical tests discussed herein.

Table 1:

Summary of new site level paleomagnetic data for the Beaver River diabase and anorthosite xenoliths. n/N: number of samples/sites analyzed and included in the site/grand mean; dec_{is} & inc_{is} : in situ mean declination and inclination for the site; dec_{tc} & inc_{tc} : tilt-corrected mean declination and inclination for the site; k: Fisher precision parameter; R: resultant vector length; α_{95} : 95% confidence limit in degrees; VGP lat/longitude of the virtual geomagnetic pole for the site; VGP lon/longitude of the virtual geomagnetic pole for the site. Full measurement level data are available within the MagIC database. <https://earthref.org/MagIC/17102/400ee0fb3-a79b-42bd-aeb9-9005a2e3b438>.

| site | lat | lon | n/N | dec_{is} | inc_{is} | dec_{tc} | inc_{tc} | k | α_{95} | VGP lat _{is} | VGP lon _{is} | VGP lat _{tc} | VGP lon _{tc} |
|-------------------------|------|-------|------|------------|------------|------------|------------|-------|---------------|-----------------------|-----------------------|-----------------------|-----------------------|
| AX1 | 47.2 | -91.4 | 8.0 | 293.3 | 42.6 | 288.8 | 54.9 | 536.0 | 2.4 | 33.4 | 180.0 | 37.1 | 193.2 |
| AX2 | 47.2 | -91.4 | 9.0 | 282.0 | 31.3 | 277.2 | 42.6 | 145.0 | 4.3 | 20.4 | 181.8 | 22.6 | 191.1 |
| AX3 | 47.6 | -90.9 | 10.0 | 290.4 | 28.2 | 285.1 | 38.6 | 69.0 | 5.9 | 24.7 | 174.5 | 25.9 | 183.7 |
| AX4 | 47.6 | -90.9 | 7.0 | 291.9 | 20.0 | 288.3 | 30.7 | 91.0 | 6.4 | 22.3 | 169.8 | 24.4 | 177.2 |
| AX5-10 | 47.6 | -90.9 | 14.0 | 286.2 | 29.1 | 280.7 | 38.1 | 269.5 | 2.5 | 22.3 | 178.1 | 22.7 | 186.5 |
| AX11 | 47.4 | -91.2 | 8.0 | 284.9 | 23.5 | 281.7 | 35.2 | 305.0 | 3.2 | 19.1 | 176.3 | 22.0 | 184.1 |
| AX12 | 47.3 | -91.3 | 6.0 | 299.9 | 42.5 | 297.3 | 55.2 | 36.0 | 11.3 | 37.8 | 175.1 | 43.0 | 188.4 |
| AX13 | 47.4 | -91.2 | 9.0 | 289.8 | 23.0 | 287.3 | 35.1 | 434.0 | 2.5 | 22.2 | 172.4 | 25.7 | 180.0 |
| AX14 | 47.3 | -91.3 | 7.0 | 296.9 | 38.2 | 293.9 | 50.8 | 256.0 | 3.8 | 33.7 | 174.5 | 38.2 | 186.1 |
| AX15 | 47.3 | -91.3 | 8.0 | 282.9 | 42.3 | 275.8 | 53.5 | 86.0 | 6.0 | 26.2 | 187.2 | 27.9 | 199.8 |
| AX16 | 47.3 | -91.3 | 8.0 | 273.7 | 39.1 | 265.8 | 49.2 | 396.0 | 2.8 | 18.5 | 191.6 | 19.0 | 202.9 |
| AX17 | 47.3 | -91.3 | 8.0 | 273.6 | 49.8 | 261.6 | 59.6 | 647.0 | 2.2 | 24.3 | 198.3 | 23.7 | 213.5 |
| AX18 | 47.3 | -91.3 | 9.0 | 283.8 | 45.5 | 276.0 | 56.9 | 535.0 | 2.2 | 28.5 | 188.7 | 30.2 | 202.8 |
| AX19 | 47.3 | -91.3 | 8.0 | 293.9 | 35.8 | 290.7 | 48.2 | 695.0 | 2.1 | 30.5 | 175.4 | 34.6 | 186.0 |
| AX20 | 47.3 | -91.3 | 5.0 | 294.5 | 44.3 | 290.0 | 56.7 | 271.0 | 4.7 | 35.1 | 180.4 | 39.0 | 194.5 |
| AX21 | 47.3 | -91.3 | 8.0 | 301.7 | 37.7 | 299.9 | 50.5 | 803.0 | 2.0 | 36.7 | 170.4 | 42.1 | 181.7 |
| AX22 | 47.4 | -91.2 | 9.0 | 297.2 | 43.1 | 293.8 | 55.7 | 208.0 | 3.6 | 36.3 | 177.6 | 41.0 | 191.1 |
| Anorthosite mean | | | | | | | | | | | | | |
| BD1 | 47.2 | -91.4 | 15.0 | 293.1 | 40.9 | 288.8 | 53.2 | 623.0 | 1.5 | 32.4 | 179.0 | 36.1 | 191.6 |
| BD2 | 47.6 | -90.9 | 8.0 | 286.6 | 22.7 | 282.0 | 32.6 | 122.0 | 5.0 | 19.9 | 175.0 | 21.0 | 182.8 |
| BD3 | 47.4 | -91.2 | 8.0 | 286.6 | 29.8 | 282.8 | 41.6 | 212.0 | 3.8 | 22.9 | 177.9 | 25.8 | 186.9 |
| BD4 | 47.3 | -91.3 | 8.0 | 300.2 | 40.7 | 297.9 | 53.4 | 47.0 | 8.2 | 37.1 | 173.6 | 42.3 | 186.0 |
| BD5 | 47.3 | -91.3 | 8.0 | 282.7 | 44.8 | 274.8 | 56.0 | 271.0 | 3.4 | 27.4 | 188.9 | 28.9 | 202.6 |
| BD6 | 47.3 | -91.3 | 9.0 | 300.0 | 33.2 | 298.3 | 46.0 | 64.0 | 6.5 | 33.4 | 169.2 | 38.6 | 178.9 |
| BD7 | 47.3 | -91.3 | 7.0 | 292.4 | 53.1 | 285.0 | 65.3 | 305.0 | 3.5 | 38.5 | 189.2 | 41.3 | 208.3 |
| BD8 | 47.2 | -91.4 | 10.0 | 287.9 | 52.8 | 278.8 | 64.5 | 300.0 | 2.8 | 35.3 | 191.8 | 37.1 | 209.9 |
| BD9 | 47.2 | -91.3 | 7.0 | 278.2 | 33.8 | 272.3 | 44.6 | 55.0 | 8.2 | 19.0 | 185.7 | 20.4 | 195.6 |
| BD10 | 47.4 | -91.2 | 10.0 | 297.0 | 46.2 | 293.0 | 58.7 | 341.0 | 2.6 | 37.8 | 180.0 | 42.2 | 195.1 |
| BD11 | 47.4 | -91.3 | 8.0 | 296.4 | 41.7 | 293.0 | 54.2 | 429.0 | 2.7 | 35.1 | 177.1 | 39.5 | 189.9 |
| BD12 | 47.3 | -91.3 | 8.0 | 288.8 | 38.1 | 284.1 | 50.1 | 141.0 | 4.7 | 28.1 | 180.4 | 31.3 | 191.8 |
| BD13 | 47.5 | -91.1 | 8.0 | 280.4 | 22.4 | 276.9 | 33.6 | 341.0 | 3.0 | 15.6 | 179.2 | 18.0 | 186.7 |
| BD15 | 47.7 | -90.6 | 8.0 | 300.1 | 2.3 | 299.3 | 14.2 | 119.0 | 5.1 | 20.6 | 156.9 | 24.8 | 161.7 |
| BD17 | 47.4 | -91.2 | 8.0 | 295.1 | 28.5 | 292.9 | 41.0 | 550.0 | 2.4 | 28.0 | 170.8 | 32.3 | 179.3 |
| Diabase mean | | | | | | | | | | | | | |
| | 15.0 | 291.0 | 35.7 | 286.9 | 47.7 | 51.6 | 5.0 | 29.0 | | 178.2 | 32.5 | 189.5 | |

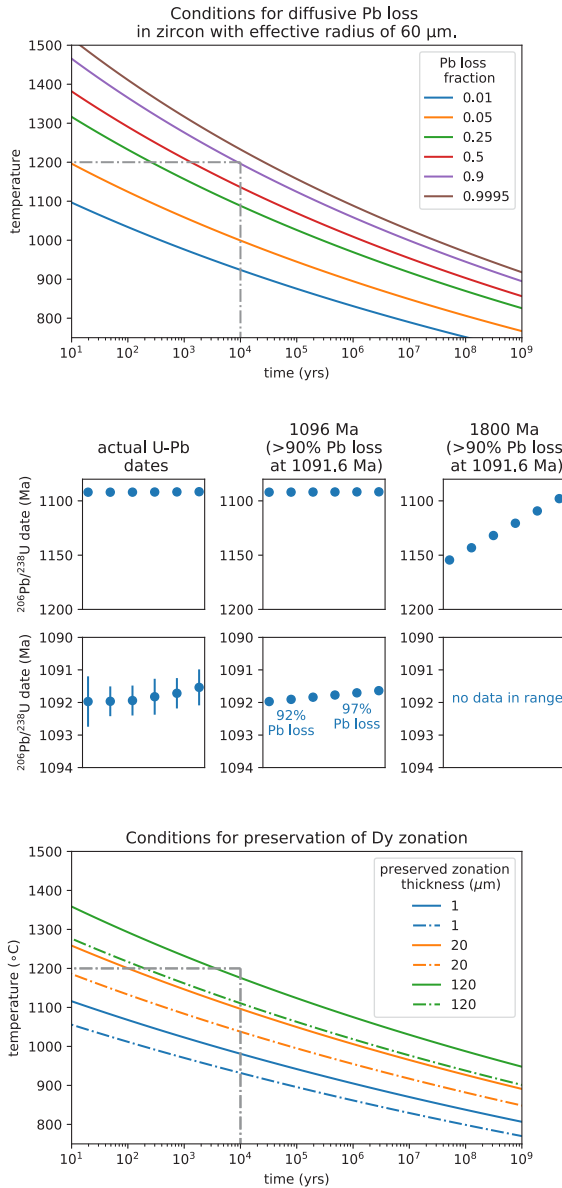


Figure 10: Top: Conditions for diffusive Pb loss in crystalline zircon for zircons of effective radii of 60 μm . Curves represent time-temperature conditions under which zircon will lose the indicated fraction of total Pb; Middle: Modeled zircon Pb loss scenarios with initial crystallization ages of 1091.8 Ma, 1096 Ma, and 1800 Ma with varying degrees of Pb loss at 1091.6 Ma compared to the actual U-Pb dates; Bottom: Conditions for preservation of Dy zoning in zircon. Curves represent time-temperature conditions under which different zoning thicknesses would be preserved in zircon. For conditions above the upper solid curves in each group, well-defined zoning will be lost at a given thickness. For conditions above the dashdot lines, zones will be partially lost but will retain initial composition in zone center. Pb diffusion and Dy zoning models follow Cherniak and Watson (2001) and Cherniak et al. (1997).

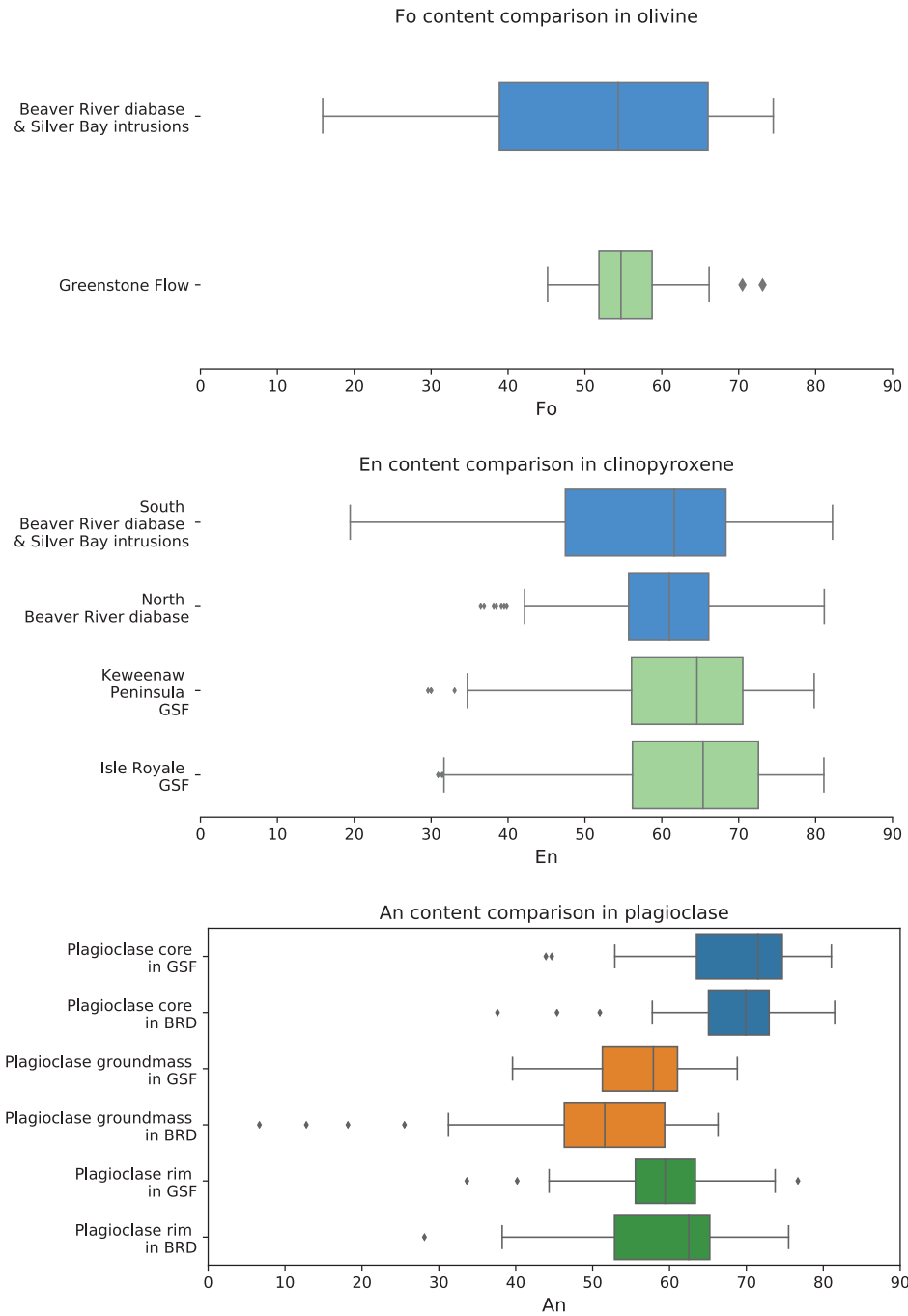


Figure 11: Box plots of geochemical analyses of olivine, pyroxene, and plagioclase in the Beaver River diabase (BRD) and Greenstone Flow (GSF). The fosterite content in olivine crystals and the enstatite content in clinopyroxene crystals are very similar in the Beaver River diabase and the Greenstone Flow. The anorthite concentrations in the core, groundmass, and rim of the plagioclase megacrysts within the Beaver River diabase and the Greenstone Flow share very similar patterns and the distributions are nearly identical. The box encloses the middle 50% of the data ranges (i.e., the interquartile range), and the notch represents the median values. The whiskers extend to the 2.5th and 97.5th percentile values. Fo-fosterite; En-enstatite; An-anorthite. Data from Doyle (2016).

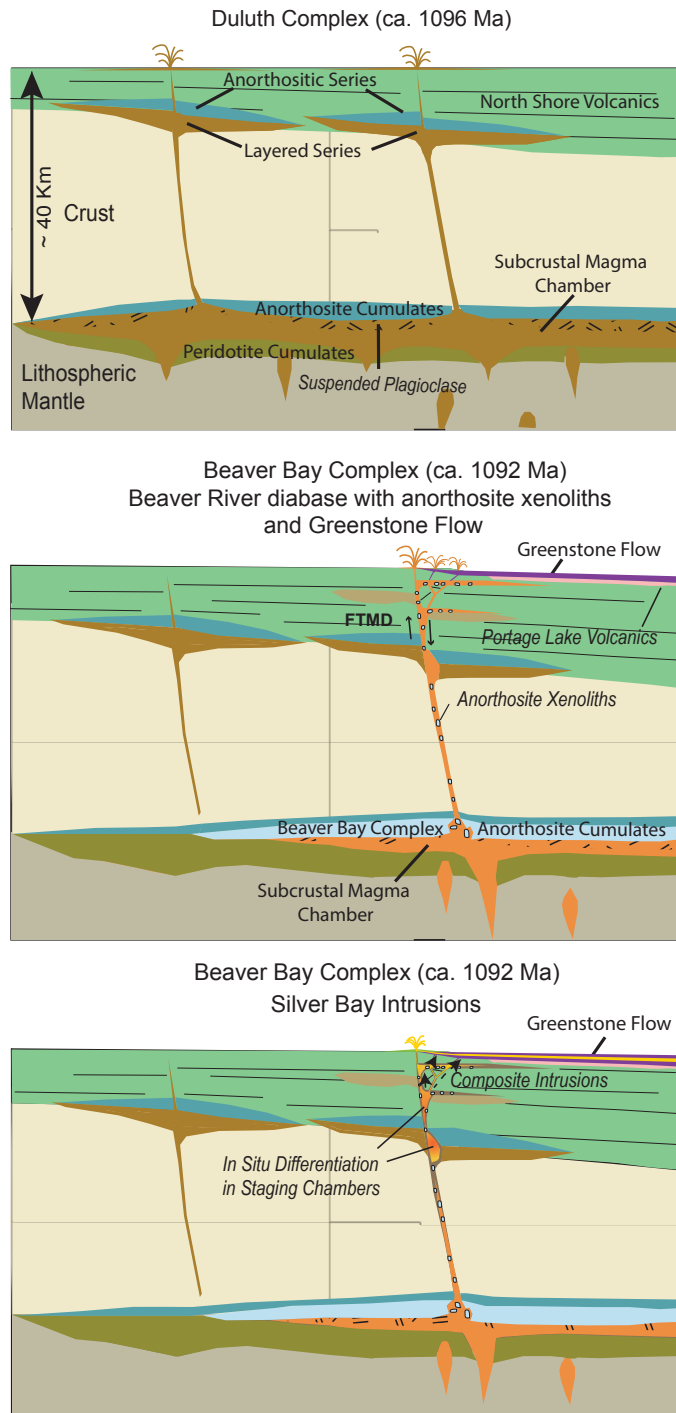


Figure 12: Schematic illustration of the emplacement of the *ca.* 1096 Ma Duluth Complex, the *ca.* 1092 Ma Beaver Bay Complex, Greenstone Flow and associated anorthositic lithologies. Top: Duluth Complex Anorthositic Series formed by subhorizontal emplacement of plagioclase crystal mushes generated by plagioclase flotation in subcrustal magma chambers. The Layered Series formed by emplacement of crystal-poor mafic magmas beneath the Anorthositic Series and variable differentiation by in situ fractional crystallization. Middle: Development of a deep crustal magma chamber that formed anorthosite cumulates and intrusion of the anorthosite xenolith-bearing Beaver River diabase of the Beaver Bay Complex along a major crustal fault (FTMD-Finland Tectonomagmatic Discontinuity) and its massive eruption at surface that could have formed the Greenstone Flow. Bottom: Emplacement of the Beaver River diabase and the Greenstone Flow. The Silver Bay intrusion may have added to the composite composition of both units, through magma differentiation in deeper staging chambers. The erosional unconformity between the Schroeder Lutzen basalt and the Beaver River diabase suggest the diabase

622 **References**

- 623 Beck, M. E. (1970). Paleomagnetism of Keweenawan Intrusive Rocks, Minnesota. *Journal of Geophysical Research*, 75(26), 4985–4996. doi: 10.1029/jb075i026p04985
- 626 Beck, M. E., & Lindsley, N. C. (1969). Paleomagnetism of the Beaver Bay Complex, Minnesota. *Journal of Geophysical Research*, 74(8), 2002–2013. doi: 10.1029/jb074i008p02002
- 628 Boerboom, T. J. (2004). *M-147 Bedrock geology of the Split Rock Point quadrangle, Lake County, Minnesota* (Tech. Rep.). Minnesota Geological Survey.
- 631 Boerboom, T. J., Green, J., & Albers, P. (2007). *M-174 Bedrock geology of the Lutzen quadrangle, Cook County, Minnesota* (Tech. Rep.). Minnesota Geological Survey.
- 633 Boerboom, T. J., & Green, J. C. (2006). *M-170 Bedrock geology of the Schroeder quadrangle, Cook County, Minnesota* (Tech. Rep.). Minnesota Geological Survey.
- 637 Boerboom, T. J., Green, J. C., Albers, P., & Miller, J., J.D. (2006). *M-171 Bedrock geology of the Tofte quadrangle, Cook County, Minnesota* (Tech. Rep.). Minnesota Geological Survey.
- 640 Books, K. G., White, W. S., & Beck, M. E. (1966). *Magnetization of Keweenawan gabbro in northern Wisconsin and its relation to time of intrusion*. Geological Survey Research.
- 643 Bryan, S. E., Peate, I. U., Peate, D. W., Self, S., Jerram, D. A., Mawby, M. R., ... Miller, J. A. (2010). The largest volcanic eruptions on Earth. *Earth-Science Reviews*, 102(3-4), 207–229. doi: 10.1016/j.earscirev.2010.07.001
- 646 Cannon, W. F., & Hinze, W. J. (1992). Speculations on the origin of the North American Midcontinent rift. *Tectonophysics*, 213(1-2), 49–55. doi: 10.1016/0040-1951(92)90251-z
- 649 Cannon, W. F., & Nicholson, S. W. (2001). Geologic map of the Keweenaw Peninsula and adjacent area, Michigan. *USGS Numbered Series*, 2696.
- 651 Cherniak, D., Hanchar, J., & Watson, E. (1997). Rare-earth diffusion in zircon. *Chemical Geology*, 134(4), 289–301. doi: 10.1016/s0009-2541(96)00098-8
- 653 Cherniak, D., & Watson, E. (2001). Pb diffusion in zircon. *Chemical Geology*, 172(1-2), 5–24. doi: 10.1016/s0009-2541(00)00233-3

- 655 Condon, D. J., Schoene, B., McLean, N. M., Bowring, S. A., & Parrish, R. R.
656 (2015, 1). Metrology and traceability of U–Pb isotope dilution geochronol-
657 ogy (EARTHTIME tracer calibration part I). *Geochimica et Cosmochimica
658 Acta*, *164*, 464–480. doi: 10.1016/j.gca.2015.05.026
- 659 Cornwall, H. R. (1951). Differentiation in lavas of the Keweenawan Series and the
660 origin of the copper deposits of Michigan. *Geological Society of America Bul-
661 letin*, *62*(2), 159. doi: 10.1130/0016-7606(1951)62[159:dilotk]2.0.co;2
- 662 Davis, D. W., & Paces, J. B. (1990). Time resolution of geologic events on the
663 Keweenaw Peninsula and implications for development of the Midcontinent
664 Rift system. *Earth and Planetary Science Letters*, *97*(1-2), 54–64. doi:
665 10.1016/0012-821x(90)90098-i
- 666 Delaney, P. (1987). *Heat transfer during emplacement and cooling of mafic dykes*.
667 Geological Association of Canada.
- 668 Doyle, M. (2016). *Geologic and geochemical attributes of the Beaver River Diabase
669 and Greenstone Flow: Testing a possible intrusive-volcanic link in the 1.1 Ga
670 Midcontinent Rift* (Unpublished master's thesis). University of Minnesota.
- 671 Fairchild, L. M., Swanson-Hysell, N. L., Ramezani, J., Sprain, C. J., & Bowring,
672 S. A. (2017). The end of Midcontinent Rift magmatism and the paleogeogra-
673 phy of Laurentia. *Lithosphere*, *9*(1), 117–133. doi: 10.1130/1580.1
- 674 Ferry, J. M., & Watson, E. B. (2007). New thermodynamic models and revised cal-
675ibrations for the Ti-in-zircon and Zr-in-rutile thermometers. *Contributions to
676 Mineralogy and Petrology*, *154*(4), 429–437. doi: 10.1007/s00410-007-0201-0
- 677 Foucher, M. (2018). *Probing the Precambrian geodynamo: analysis of the geomag-
678 netic field behavior and calibration of pseudo-thellier paleointensity method for
679 Mesoproterozoic rocks* (Unpublished doctoral dissertation). Michigan Techno-
680 logical University.
- 681 Green, J. C. (1982). 5: Geology of Keweenawan extrusive rocks. *Geological Society
682 of America Memoirs*, *156*, 47–56.
- 683 Grout, S. G. M., Frank F. (1939). The geology of the anorthosites of the Minnesota
684 coast of Lake Superior. Minnesota Geological Survey.
- 685 Heaman, L. M., Easton, R. M., Hart, T. R., Hollings, P., MacDonald, C. A., &
686 Smyk, M. (2007). Further refinement to the timing of Mesoproterozoic mag-
687 matism, Lake Nipigon region, Ontario. *Canadian Journal of Earth Sciences*,

- 688 44(8), 1055–1086. doi: 10.1139/e06-117
- 689 Hinze, W. J., & Chandler, V. W. (2020). Reviewing the configuration and extent
690 of the Midcontinent Rift system. *Precambrian Research*, 342, 105688. doi: 10
691 .1016/j.precamres.2020.105688
- 692 Huber, N. (1973). *The Portage Lake Volcanics (Middle Keweenawan) on Isle
693 Royale, Michigan* (Tech. Rep.). United States Geological Survey.
- 694 Jirsa, M. A., Boerboom, T., Chandler, V., Mossler, J., Runkel, A., & Setterholm,
695 D. (2011). *S-21 Geologic map of Minnesota-bedrock geology* (Tech. Rep.).
696 Minnesota Geological Survey.
- 697 Kushiro, I. (1980). Viscosity, density, and structure of silicate melts at high pres-
698 sures, and their petrological applications. *Physics of magmatic processes*, 93-
699 120.
- 700 Lane, A. C. (1911). The Keweenaw series of Michigan. *Michigan Geological and Bio-
701 logical Survey Publication 6*, 2(4), 983.
- 702 Lawson, A. C. (1893). The anorthosites of the Minnesota Coast of Lake Superior:
703 Geological and Natural History Survey of Minnesota. *Bulletin*, 8, 1-23.
- 704 Longo, A. A. (1984). *A correlation for a middle Keweenawan flood basalt: the
705 Greenstone flow, Isle Royale and Keweenaw Peninsula, Michigan* (Unpublished
706 master's thesis). Michigan Technological University.
- 707 Mattinson, J. M. (2005). Zircon U-Pb chemical abrasion (“CA-TIMS”) method:
708 Combined annealing and multi-step partial dissolution analysis for improved
709 precision and accuracy of zircon ages. *Chemical Geology*, 220(1-2), 47–66. doi:
710 10.1016/j.chemgeo.2005.03.011
- 711 McFadden, P., & McElhinny, M. (1990). Classification of the reversal test in palaeo-
712 magnetism. *Geophysical Journal International*, 103, 725-729.
- 713 Miller, J., J.D. (1988). *M-065 Geologic map of the Silver Bay and Split Rock Point
714 NE quadrangles, Lake County, Minnesota* (Tech. Rep.).
- 715 Miller, J., J.D., & Boerboom, T. J. (1989). *M-066 geologic map of the Illgen City
716 quadrangle, Lake County, Minnesota* (Tech. Rep.). Minnesota Geological Sur-
717 vey.
- 718 Miller, J., J.D., Boerboom, T. J., & Jerde, E. (1994). *M-082 Bedrock geologic map of
719 the Cabin Lake and Cramer quadrangles, Lake and Cook Counties, Minnesota*
720 (Tech. Rep.). Minnesota Geological Survey.

- 721 Miller, J., J.D., & Chandler, V. W. (1997). Geology, petrology, and tectonic signifi-
722 cance of the Beaver Bay Complex, northeastern Minnesota. In *Middle Protero-*
723 *zoic to Cambrian rifting, central North America.* Geological Society of Amer-
724 ica. doi: 10.1130/0-8137-2312-4.73
- 725 Miller, J., J.D., & Nicholson, S. W. (2013). Geology and Mineral Deposits of the 1.1
726 Ga Midcontinent Rift in the Lake Superior Region – An Overview. In *Field*
727 *guide to the copper-nickel-platinum group element deposits of the lake superior*
728 *region.* Precambrian Research Center.
- 729 Miller, J., J.D., Severson, M. J., Chandler, V. W., & Peterson, D. M. (2001). *M-119*
730 *Geologic map of the Duluth Complex and related rocks, northeastern Minnesota*
731 (Tech. Rep.). Minnesota Geological Survey.
- 732 Miller, J., J.D., & Weiblen, P. W. (1990). Anorthositic rocks of the Duluth Com-
733 plex: Examples of rocks formed from plagioclase crystal mush. *Journal of*
734 *Petrology*, 31(2), 295–339. doi: 10.1093/petrology/31.2.295
- 735 Morrison, D. A., Ashwal, L. D., Phinney, W. C., Shih, C.-Y., & Wooden, J. L.
736 (1983). Pre-Keweenawan anorthosite inclusions in the Keweenawan Beaver Bay
737 and Duluth Complexes, northeastern Minnesota. *Geological Society of America*
738 *Bulletin*, 94(2), 206. doi: 10.1130/0016-7606(1983)94<206:paikit>2.0.co;2
- 739 Paces, J. B., & Miller, J., J.D. (1993). Precise U-Pb ages of Duluth Complex and
740 related mafic intrusions, northeastern Minnesota: Geochronological insights
741 to physical, petrogenetic, paleomagnetic, and tectonomagmatic processes as-
742 sociated with the 1.1 Ga Midcontinent Rift System. *Journal of Geophysical*
743 *Research: Solid Earth*, 98(B8), 13997–14013. doi: 10.1029/93jb01159
- 744 Reidel, S. P., Camp, V. E., Tolan, T. L., & Martin, B. S. (2013). The Columbia
745 River flood basalt province: Stratigraphy, areal extent, volume, and physical
746 volcanology. In *The Columbia River Flood Basalt Province.* Geological Society
747 of America. Retrieved from
- 748 Remond, G., Cesbron, F., Chapoulie, R., Ohnenstetter, D., Roques-Carmes, C.,
749 & Schvoerer, M. (1992). Cathodoluminescence applied to the microchar-
750 acterization of mineral materials: a present status in experimentation and
751 interpretation. *Scanning microscopy*, 6(1), 2.
- 752 Rubatto, D. (2002). Zircon trace element geochemistry: partitioning with garnet and
753 the link between U–Pb ages and metamorphism. *Chemical Geology*, 184(1-2),

- 754 123–138. doi: 10.1016/s0009-2541(01)00355-2
- 755 Schaltegger, U., Fanning, C. M., Günther, D., Maurin, J. C., Schulmann, K., &
756 Gebauer, D. (1999). Growth, annealing and recrystallization of zircon
757 and preservation of monazite in high-grade metamorphism: conventional
758 and in-situ U-Pb isotope, cathodoluminescence and microchemical evi-
759 dence. *Contributions to Mineralogy and Petrology*, 134(2-3), 186–201. doi:
760 10.1007/s004100050478
- 761 Schmitz, M. D., Bowring, S. A., & Ireland, T. R. (2003). Evaluation of Duluth
762 Complex anorthositic series (AS3) zircon as a U-Pb geochronological stan-
763 dard: new high-precision isotope dilution thermal ionization mass spectrom-
764 etry results. *Geochimica et Cosmochimica Acta*, 67(19), 3665–3672. doi:
765 10.1016/s0016-7037(03)00200-x
- 766 Schoene, B., Crowley, J. L., Condon, D. J., Schmitz, M. D., & Bowring, S. A.
767 (2006). Reassessing the uranium decay constants for geochronology using
768 ID-TIMS U–Pb data. *Geochimica et Cosmochimica Acta*, 70(2), 426–445. doi:
769 10.1016/j.gca.2005.09.007
- 770 Self, S., Jay, A., Widdowson, M., & Keszthelyi, L. (2008). Correlation of the Deccan
771 and Rajahmundry Trap lavas: Are these the longest and largest lava flows on
772 Earth? *Journal of Volcanology and Geothermal Research*, 172(1-2), 3–19. doi:
773 10.1016/j.jvolgeores.2006.11.012
- 774 Shank, S. G. (1989). The petrology of the Beaver Bay Complex near Silver Bay,
775 northeastern Minnesota. *Minnesota, University of Minnesota*.
- 776 Stewart, E. K., Grauch, V., Woodruff, L., & Heller, S. (2018). Seismic stratigraphy
777 of the 1.1 Ga Midcontinent Rift beneath western Lake Superior Part II: Evolu-
778 tion of rift-fill through time. In *GSA Annual Meeting in Indianapolis, Indiana,*
779 *USA-2018*.
- 780 Sun, S.-S., & McDonough, W. F. (1989). Chemical and isotopic systematics of
781 oceanic basalts: implications for mantle composition and processes. *Geological
782 Society, London, Special Publications*, 42(1), 313–345. doi: 10.1144/gsl.sp.1989
.042.01.19
- 783 Swanson-Hysell, N. L., Hoaglund, S. A., Crowley, J. L., Schmitz, M. D., Zhang,
784 Y., & Miller, J. D. (2020). Rapid emplacement of massive Duluth Com-
785 plex intrusions within the North American Midcontinent Rift. *Geology*. doi:
786

- 787 10.1130/g47873.1
- 788 Swanson-Hysell, N. L., Maloof, A. C., Weiss, B. P., & Evans, D. A. D. (2009).
- 789 No asymmetry in geomagnetic reversals recorded by 1.1-billion-year-old Ke-
- 790 weenawan basalts. *Nature Geoscience*, 2(10), 713–717. doi: 10.1038/ngeo622
- 791 Swanson-Hysell, N. L., Ramezani, J., Fairchild, L. M., & Rose, I. R. (2019). Failed
- 792 rifting and fast drifting: Midcontinent Rift development, Laurentia's rapid mo-
- 793 tion and the driver of Grenvillian orogenesis. *GSA Bulletin*, 131(5-6), 913–940.
- 794 doi: 10.1130/b31944.1
- 795 Tauxe, L., Shaar, R., Jonestrask, L., Swanson-Hysell, N. L., Minnett, R., Koppers,
- 796 A. A. P., . . . Fairchild, L. (2016). PmagPy: Software package for paleomag-
- 797 netic data analysis and a bridge to the Magnetics Information Consortium
- 798 (MagIC) Database. *Geochemistry, Geophysics, Geosystems*, 17(6), 2450–2463.
- 799 doi: 10.1002/2016gc006307
- 800 Unsworth, J., & Duarte, F. J. (1979). Heat diffusion in a solid sphere and Fourier
- 801 theory: An elementary practical example. *American Journal of Physics*,
- 802 47(11), 981–983. doi: 10.1119/1.11601
- 803 van Hinsbergen, D. J. J., Steinberger, B., Doubrovine, P. V., & Gassmöller, R.
- 804 (2011). Acceleration and deceleration of India-Asia convergence since the
- 805 Cretaceous: Roles of mantle plumes and continental collision. *Journal of*
- 806 *Geophysical Research*, 116(B6). doi: 10.1029/2010jb008051
- 807 Vervoort, J. D., Wirth, K., Kennedy, B., Sandland, T., & Harpp, K. S. (2007). The
- 808 magmatic evolution of the Midcontinent rift: New geochronologic and geo-
- 809 chemical evidence from felsic magmatism. *Precambrian Research*, 157(1-4),
- 810 235–268. doi: 10.1016/j.precamres.2007.02.019
- 811 White, W. (1960). The Keweenawan lavas of Lake Superior, an example of flood
- 812 basalts. *American Journal of Science*, 258, 367–374.